Development/Plasticity/Repair

Molecular Characterization of Nodose Ganglia Development Reveals a Novel Population of Phox2b+ Glial Progenitors in Mice

Elijah D. Lowenstein,[1,2]* Aristotelis Misios,[1,2,3]* Sven Buchert,[1,2] and Pierre-Louis Ruffault[1,2]

[1]Developmental Biology/Signal Transduction, Max Delbrück Center for Molecular Medicine, Berlin 13125, Germany, [2]NeuroCure Cluster of Excellence, Charité-Universitätsmedizin Berlin, Corporate Member of Freie Universität Berlin and Humboldt-Universität zu Berlin, Berlin 10117, Germany, and [3]Systems Biology of Gene Regulatory Elements, Berlin Institute for Medical Systems Biology, Max Delbrück Center for Molecular Medicine, Berlin 10115, Germany

The vagal ganglia, comprised of the superior (jugular) and inferior (nodose) ganglia of the vagus nerve, receive somatosensory information from the head and neck or viscerosensory information from the inner organs, respectively. Developmentally, the cranial neural crest gives rise to all vagal glial cells and to neurons of the jugular ganglia, while the epibranchial placode gives rise to neurons of the nodose ganglia. Crest-derived nodose glial progenitors can additionally generate autonomic neurons in the peripheral nervous system, but how these progenitors generate neurons is unknown. Here, we found that some Sox10+ neural crest-derived cells in, and surrounding, the nodose ganglion transiently expressed Phox2b, a master regulator of autonomic nervous system development, during early embryonic life. Our genetic lineage-tracing analysis in mice of either sex revealed that despite their common developmental origin and extreme spatial proximity, a substantial proportion of glial cells in the nodose, but not in the neighboring jugular ganglia, have a history of Phox2b expression. We used single-cell RNA–sequencing to demonstrate that these progenitors give rise to all major glial subtypes in the nodose ganglia, including Schwann cells, satellite glia, and glial precursors, and mapped their spatial distribution by in situ hybridization. Lastly, integration analysis revealed transcriptomic similarities between nodose and dorsal root ganglia glial subtypes and revealed immature nodose glial subtypes. Our work demonstrates that these crest-derived nodose glial progenitors transiently express Phox2b, give rise to the entire complement of nodose glial cells, and display a transcriptional program that may underlie their bipotent nature.

Key words: peripheral glia; development; neural crest; nodose; Phox2b; vagal ganglia

Significance Statement

The nodose ganglia contain sensory neurons that innervate inner organs and play key roles in homeostatic behaviors like digestion, regulation of blood pressure and heart rate, and breathing. Nodose sensory neurons are supported by nodose glial cells, which are understudied compared with their neuronal neighbors. Specifically, the genetic program governing their development is not fully understood. Here, we uncover a transcriptional program unique to nodose glial cells (transient expression of Phox2b) that resolves the 40-year-old finding that nodose glial progenitors can also give rise to autonomic neurons (whose development depends on Phox2b expression). Lastly, we leveraged single-cell RNA–sequencing to identify four major subtypes of nodose glial cells and used subtype-specific marker genes to map their spatial distribution.

Introduction

Viscerosensory neurons in the nodose ganglia are important to maintain bodily homeostasis and reside intermingled with resident peripheral glial cells (Chang et al., 2015; Zeng et al., 2018; Vermeiren et al., 2020; Prescott and Liberles, 2022; Lowenstein et al., 2023). Peripheral glial cells, including both Schwann cells and satellite glia (SG), regulate synaptic connectivity and provide nutrients and structural support, as well as myelinate neurons in the peripheral nervous system (Riethmacher et al., 1997; Véga et al., 2003; Hanani, 2005; Fields and Burnstock, 2006; Jessen et al., 2015; Monk et al., 2015; Avraham et al., 2020). Single-cell RNA–sequencing (scRNA-seq) has begun to elucidate the diversity of peripheral glial cells in numerous peripheral nerves as well as in autonomic and somatosensory ganglia, revealing transcriptomic differences in glial cell types across the peripheral nervous system (Wolbert et al., 2020; Gerber et al., 2021; Tasdemir-Yilmaz et al., 2021; Avraham et al., 2022; Mapps et al., 2022b). However, the number of glial types in the viscerosensory nodose ganglia and their transcriptomic profiles that support the vast array of nodose neuron types is not known.

Developmentally, cells of the nodose ganglia arise from two neurogenic niches: glial cells derive from the cranial neural crest, while neurons derive from the epibranchial placode (Vermeiren et al., 2020). The differential contributions of the crest and placode were elucidated by a series of seminal quail–chick embryo transplantation studies where isotropic and isochronic grafts of quail crest or placode were transplanted into a chick host (Narayanan and Narayanan, 1980; Ayer-Le Lievre and Le Douarin, 1982; D'amico-Martel and Noden, 1983). These chimeras demonstrated that crest-derived non–neuronal nodose cells could generate autonomic neurons when back-transplanted into the neural crest of a younger host (Ayer-Le Lievre and Le Douarin, 1982; Le Douarin, 1986; Fontaine-Perus et al., 1988; Douarin et al., 1991). Although crest derivatives only generate glial cells in the nodose ganglia, they may acquire other cell fates when placed in a new permissive environment.

In mice the viscerosensory nodose ganglia, i.e., inferior ganglia of the vagus nerve, are directly abutting the somatosensory jugular ganglia, i.e., superior ganglia of the vagus nerve. In contrast to the nodose ganglia, both neurons and glial cells of the jugular ganglia derive from the cranial neural crest (Vermeiren et al., 2020). Thus, the same neurogenic niche generates both jugular and nodose glial cells, but it is currently unknown whether there are molecular differences between nodose and jugular glial cell development.

With the advent of molecular biology and the development of genetic lineage tracing, the broad transcriptional programs necessary for peripheral glial cell and neuron development were revealed. All peripheral glial cells derive from the neural crest, an embryonic niche that depends on the Wnt signaling pathway (Jessen and Mirsky, 2005; Jacob, 2015; Erickson et al., 2023). The successful differentiation of neural crest cells into the full complement of peripheral glial cells relies on the transcription factor *Sox10*, whose ablation precludes the generation of Schwann cells and satellite glia (SG) (Kuhlbrodt et al., 1998; Britsch et al., 2001). In contrast, neurons of the autonomic nervous system, including sympathetic, parasympathetic, enteric, and cranial sensory neurons, depend on the related homeobox transcription factors *Phox2a* and *Phox2b* for their development and maintenance (Pattyn et al., 1997, 1999; Yang et al., 2002). Thus, transgenic mouse strains expressing recombinases in cells expressing *Wnt1* and *Phox2b* provide tools to study crest and placode derivatives, respectively.

Despite the fact that Phox2a/b instruct neuronal fates, in parasympathetic preganglionic nerves, some nerve-associated Sox10+ glial precursors (GPs) transiently express Phox2b before adopting a mature Schwann cell identity (Dyachuk et al., 2014; Espinosa-Medina et al., 2014). Recent studies used scRNA-seq to dissect the transcriptional changes coinciding with cell fate acquisition and found that many cells initially express competing gene modules (e.g., neuronal and glial), before selecting one module over the other (e.g., neuronal > glial; Soldatov et al., 2019; Kastriti et al., 2022). However, whether the bipotent nature of nodose glial cells revealed by the early quail–chick transplantation experiments is reflected in their transcriptional program during development remains to be investigated. Specifically, we hypothesize that one should be able to find nodose glial cells that transiently express Phox2b, the master transcription factor that is required for proper autonomic neuron development.

Here, we used genetic lineage tracing and scRNA-seq to identify the transcriptional programs leading to the development of neurons and glial cells in the nodose ganglia. We show that a significant proportion of nodose, but not jugular, glial cells derive from a subset of Wnt1+ neural crest progenitors that transiently express Phox2b during early embryogenesis. Our scRNA-seq results revealed the developmental potential of neural crest cells that have a history of Phox2b expression to include all major glial subtypes, that is, myelinating (MSCs) and nonmyelinating Schwann cells (NMSCs), but also SG and GPs. These results suggest that the bipotent character of nodose glial cell progenitors is reflected in their transcriptional program and differentiates them from jugular glial cell progenitors despite their shared developmental origins and spatial proximity.

Materials and Methods

Mouse lines. All experiments were conducted according to regulations established by the Max Delbrück Center for Molecular Medicine (Landesamt für Gesundheit und Soziales). Ai14 (#007914) and Ai65 (#021875) mice were obtained from the Jackson Laboratory (Madisen et al., 2010, 2015). Tau$^{nLacZ-mGFP}$ (Hippenmeyer et al., 2005) mice were provided by Silvia Arber (Biozentrum, University of Basel). Wnt1^{Cre} (Danielian et al., 1998) mice were provided by Andrew McMahon (University of Southern California). Phox2b^{Cre} (D'Autréaux et al., 2011) and Phox2b^{FlpO} (Hirsch et al., 2013) mice were provided by Jean-François Brunet (Institut de Biologie de l'ENS). R26$^{ds-nGFP}$ (Stam et al., 2012) mice were provided by Martyn Goulding (Salk Institute for Biological Studies). Gt(ROSA)26Sor<tm2.1Sia> mice were provided by Shinichi Aizawa (RIKEN Center for Developmental Biology); we refer to them as R26^{nGFP} mice, as they express a nuclear GFP upon cre-mediated stop cassette excision (Abe et al., 2011). Mice were housed at room temperature (23°C) and 56% humidity and with a 12 h light/dark cycle.

Tissue processing. Pregnant dams were staged using the presence of a vaginal plug. The day that a vaginal plug was visible was designated as Embryonic Day (E) 0.5. Embryos were delivered by cesarean section and fixed for 1–3 h in 4% PFA in PBS at 4°C. They were washed for 2 × 10 min in PBS at room temperature before cryopreservation overnight at 4°C in 15% sucrose in PBS and then overnight at 4°C in 30% sucrose in PBS. Cryopreserved embryos were washed once and embedded in Tissue-Tek O.C.T. (Sakura Finetek) in a plastic block before being stored at −80°C. Embryos were sectioned at 20 µm using a cryostat. Vagal ganglia were dissected from Postnatal Day (P) 4 pups and fixed for 1 h in 4% PFA in PBS, before cryopreservation for 30 min in 15% sucrose in PBS followed by 30 min in 30% sucrose in PBS all at 4°C. Vagal ganglia were washed once and embedded in Tissue-Tek O.C.T. (Sakura Finetek) in a plastic block before being stored at −80°C. Vagal ganglia were sectioned at 16 µm using a cryostat. After sectioning, slides were stored at −80°C until further use.

Immunofluorescence. Immunofluorescence experiments were performed on cryosections using the following primary antibodies: rat anti-GFP (Nacalai Tesque, GF090R, 1:1,000), goat anti-Phox2b (R&D Systems, AF4940, 1:200), rabbit anti-Sox10 (Abcam, ab227680, 1:200), goat anti-Sox10 (R&D Systems, AF2864, 1:200), guinea pig anti-Tlx3 (1:5,000, kindly provided by Thomas Müller; Müller et al., 2005), goat anti-TrkA (R&D Systems, AF175, 1:500), goat anti-TrkB (R&D Systems, AF1494, 1:300), chicken anti-βgal (Abcam, ab134435, 1:1,000), chicken anti-GFP (Aves Labs, GFP-1020, 1:500), rabbit anti-RFP (Rockland Immunochemicals, 600-401-379-RTU, 1:500), goat anti-RFP (Biorbyt, orb334992, 1:500), and rabbit anti-Phox2b (1:500, kindly provided by Jean-François Brunet). Slides were removed from −80°C and thawed at 37°C for 30 min. Slides were washed once in PBS for 1 min and once in PBX (PBS with 0.2% Triton X-100) for 3 min at room temperature. Sections were then incubated in blocking solution (PBX with 5% horse serum) for 1 h at room temperature. Primary antibodies were diluted in blocking solution and left on the sections overnight at room temperature. Slides were then washed twice in PBS for 30 s, twice in PBS for 10 min, and once in PBX for 10 min at room temperature. Species-specific secondary antibodies coupled to Cy2, Cy3, or Cy5 (Jackson ImmunoResearch Laboratories, 1:500) and DAPI were diluted in blocking solution and left on the sections for 1 h at room temperature. Slides were washed three times in PBS for 10 min at room temperature before mounting them with Immu-Mount (Thermo Fisher Scientific). Please see Table 3 for a list of all antibodies used, what cell types they label, and stage analyzed.

Vagal ganglia dissociation, neuronal depletion, and cell sorting. Vagal ganglia were dissected from 4 *Phox2b^Cre;Ai14* mice at P4 of either sex and placed into ice-cold Ringer's solution (0.125 M sodium chloride, 1.5 mM calcium chloride dihydrate, 5 mM potassium chloride, 0.8 mM sodium phosphate dibasic). Ganglia were transferred to a 1.5 ml Eppendorf tube with 1.5 ml HBSS without calcium, magnesium, and phenol red (Thermo Fisher Scientific), 3 μl saturated NaHCO$_3$, 1 mg L-cysteine, and 60 U papain (Sigma-Aldrich), placed at 37°C and shaken gently for 12 min. The 1.5 ml Eppendorf tube was centrifuged at 300 RCF, and the solution was discarded, taking care not to disturb the ganglia. A prewarmed (37°C) enzyme solution containing 1 ml HBSS without calcium, magnesium, and phenol red (Thermo Fisher Scientific), 4 mg Collagenase NB4 (SERVA Electrophoresis), and 4.6 mg Dispase II (Invitrogen) was added to the ganglia, placed at 37°C, and shaken gently for 12 min. The 1.5 ml Eppendorf tube was centrifuged at 300 RCF, and the solution was discarded, taking care not to disturb the ganglia. Prewarmed (37°C) 0.5 ml HBSS without calcium, magnesium, and phenol red (Thermo Fisher Scientific) was added to the ganglia, which were triturated with a 1 ml plastic pipette tip until the ganglia began to dissociate and then with a 200 μl plastic pipette tip until the ganglia were completely dissociated. The dissociated ganglia were passed twice through a 40 μm filter (Falcon) and DAPI (Sigma-Aldrich) was added to a final concentration of 300 nM to label dead cells before sorting. We sorted tdTomato-positive/DAPI-negative cells into four 96-well plates using an ARIA Sorter III (BD Biosciences) and BD FACSDiva software 8.0.1.

A 96-well plate preparation. To prepare a master mix for 10 96-well plates, mix 26.4 μl of 10% Triton X-100, 44 μl of 25 mM dNTPs, 11 μl of 1:10,000 ERCC spike-in (ERCC spike-in/cell is 1 μl; 1:1,000,000 dilution), and 1,018.6 μl of H2O for a total of 1,100 μl. Add 10 μl per well into a master mix 96-well plate, and then add 2 μl of the barcoded primer (1 μM, 25 ng/μl) into the corresponding well. Spin down the plate at 4°C, gently vortex, and spin down again at 4°C. Carefully pipette 1.2 μl from each well of the master mix 96-well plate into the corresponding wells of the 96-well plates, spin down at 4°C, and store at −80°C.

RNA amplification. RNA amplification was done following the CEL-Seq2 protocol (Hashimshony et al., 2016). Briefly, following reverse transcription [0.4 μl first-strand buffer (five times), 0.2 μl of 0.1M DTT, 0.1 μl RNaseOUT, 0.1 μl SSII per well] and second-strand synthesis (7 μl H2O, 2.31 μl second-strand buffer, 0.23 μl of 10 mM dNTPs, 0.08 μl

E. coli DNA ligase, 0.3 μl *E. coli* DNA polymerase I, 0.08 μl RNase H per well), we pooled the contents of each well per 96-well plate into one 1.5 ml Eppendorf tube and performed bead purification with AMPure XP beads (Beckman Coulter). Next we performed in vitro transcription (Ambion), amplified RNA (aRNA) fragmentation (New England Biolabs), bead purification with RNAClean XP beads (Beckman Coulter) and eluted in 7 μl H2O. We confirmed the amount and quality of our aRNA by analyzing 1 μl of our aRNA from each 96-well plate on an RNA Pico chip with a Bioanalyzer (Agilent).

cDNA library generation. Briefly, we used the Bioanalyzer results from the RNA amplification to calculate the volume needed to obtain 5 ng aRNA from each 96-well plate and adjusted the volume to 5 μl with H2O. Next we primed the samples (1 μl random-hex RT-primer CS2, 0.5 μl of 10 mM dNTPs per sample, and incubated the samples for 5 min at 65°C), before performing reverse transcription [2 μl first-strand buffer (five times), 1 μl of 0.1 M DTT, 0.1 μl RNaseOUT, 0.1 μl SSII per well], followed by library PCR [10 μl Phusion HF Buffer (five times), 1 μl of 10 mM dNTPs, 2 μl of RPI1 primer (Illumina), 2 μl of RPIX primer (Illumina), 0.5 μl Phusion DNA Polymerase, 24.5 μl H2O per sample] and bead purification with AMPure XP beads (Beckman Coulter) and eluted in 13 μl H2O. cDNA concentration was measured using a Qubit 4 Fluorometer (Thermo Fisher Scientific), and fragment length was measured using a high-sensitivity DNA chip with a Bioanalyzer (Agilent).

Sequencing. cDNA libraries were prepared for four 96-well plates, pooled together, and sequenced on one lane of a HiSeq 1,500 (Ilumina) by the next-generation sequencing core facility at the Max Delbrück Center for Molecular Medicine. Due to the CEL-Seq2 protocol, we sequenced 16 base pairs (bp) in Read 1, 8 bp in the index, and 51 bp in Read 2 using the paired-sequencing mode.

The sequencing dataset generated in this study has been deposited in the Gene Expression Omnibus (GEO) repository (GEO accession number GSE237947) and is publicly available.

Analysis of the P4 vagal ganglia CEL-Seq2 data. Data processing and gene quantification were performed using dropseq-tools v2.0 and picard-tools v2.18.17. We used the standard pipeline for Drop-seq data, with the necessary adaptations to analyze the CEL-Seq2 data. We removed the bead barcode correction steps, and in the DigitalExpression quantification, we inputted the list of 96 CEL-Seq2 barcodes. Alignment was performed with STAR v2.5.3a (Dobin et al., 2013). We used the GRCm38 genome and the annotation from the GRCm38.p4 assembly. One cell barcode was missing from all plates, likely due to an error during library preparation, resulting in the loss of four cells. Two thresholds were set to filter out wells without cells or with damaged cells. We set a lower threshold of 5,000 UMIs (unique molecular identifiers) per cell and a lower threshold for genes detected at 200 genes per cell. After quality control, we removed 89 + 4 = 93 cells (24% of the total cell count), leaving 291 cells for downstream analyses. Downstream analyses were performed with Seurat v4.3 (Hao et al., 2021). Seurat was run with the default parameters with the following exceptions. After performing principal component analysis (PCA) and consulting the jackstraw test and standard deviation (SD) results, the first 11 principal components (PCs) were selected for downstream analysis. Upon further annotation and close inspection of the remaining PCs, PC5, PC6, and PC9 were excluded as they were driven by outlier cells. Next, the neighbor graph was constructed with FindNeighbors with a *k* parameter of 15. The clustering resolution was set to 0.8, and upon further marker gene analysis, three pairs of subtypes were collapsed, resulting in four subtypes. Uniform manifold approximation and projection (UMAP) visualization was used with the correlation metric and 15 as the number of neighbors.

Integration. The scRNA-seq dataset from Tasdemir-Yilmaz et al. (2021) was kindly provided to us by the authors in a Conos format. The whole dataset consists of seven samples from the dorsal root ganglia (DRG), spiral ganglia, and sciatic nerve, sampled across different developmental stages. We extracted and used their raw data, annotation, and two-dimensional embedding. We used Seurat v4.3 (Hao et al., 2021) and

performed canonical correlation analysis (CCA) to integrate all eight samples [the seven samples from Tasdemir-Yilmaz et al. (2021) together with our scRNA-seq dataset], using 15 canonical components. After integration, the standard analysis pipeline was performed, and the first 15 PCs of the corrected data were used to execute clustering and UMAP. Clustering resolution was set to 0.5. The rest of the integration pipeline was run using Seurat's default parameters.

We also performed cell-type label transfer, predicting which subtype annotation our cells would fall under in the new dataset, thus using it as a reference. To do this, we first integrated the dataset of Tasdemir-Yilmaz et al. (2021), as it consisted of seven different samples. Then, we used the corrected data as a reference. To find anchors for the label transfer, the PCA reduction method was used in both reference and query datasets. For the anchors as well as for the transferring of the reference labels, the first 15 PCs were used.

Single-molecule fluorescent in situ hybridization (RNAscope) and immunohistology. Single-molecule in situ fluorescent hybridization (smFISH) was performed using the RNAscope Multiplex Fluorescent Reagent Kit v2 from ACDBio according to the manufacturer's instructions. Briefly, 16-μm-thick vagal ganglion sections were thawed at 37°C for 30 min and postfixed in 4% PFA in PBS for 15 min before washing in PBS and continuing with the manufacturer's instructions. For combining immunohistology with RNAscope, we proceeded until the hydrogen peroxide wash and then washed the sections in PBS and incubated them at 4°C overnight with the primary antibody diluted in Co-detection Antibody Diluent (obtained from ACDBio). The sections were washed in PBS, and the protease treatment was performed using Protease III. The RNAscope protocol was then continued; the sections were washed in PBS and incubated with the secondary antibody for 1 h at room temperature in blocking solution (PBS with 0.2% Triton X-100 and 5% normal horse serum). Sections were washed in PBS and mounted with ProLong Gold Antifade Mountant (Thermo Fisher Scientific). We used the following probes in this study: Phox2b (407861-C2 and 407861-C3), Sox8 (454781-C2), Sox10 (435931), Scn7a (548561), Fabp7 (414651), Pou3f1 (436421-C2), and MKi67 (416771-C2). Please see Table 3 for a list of all RNAscope probes used, what cell types they label, and stage analyzed.

Microscopy, image analysis, and cell quantifications. Photomicrographs were acquired using an LSM 700 laser scanning confocal microscope (Carl Zeiss) with a 20× objective. Some images were acquired using the tile-scan mode with a 15% overlap between tiles and stitched using the ZEN 2012 software. Brightness and contrast were adjusted using ImageJ on the entire photomicrograph. Cell counts were performed by hand in ImageJ using the multipoint tool in a nonblind manner on nonconsecutive sections. Between 2 and 10 sections were counted per animal per experiment.

Statistics. Statistics were calculated using Prism 6 (GraphPad Software). Data are plotted as scatter dot plots with the mean of each animal displayed as a dot and the SD shown. Statistical significance between group means was calculated either using a two-tailed t test (two groups, Fig. 3) or a one-way analysis of variance followed by Tukey's post hoc test (>2 groups, Fig. 1).

Results

A fraction of nodose ganglia cells coexpress Sox10 and Phox2b during early embryonic development

Cells derived from the cranial neural crest (Wnt1+) and epibranchial placodes (Phox2a+) generate the glial cells and neurons of the nodose ganglia, respectively (Ayer-Le Lievre and Le Douarin, 1982; Morin et al., 1997; Pattyn et al., 1997; Dorsky et al., 1998). Interestingly, previous work showed that nodose glial cells retain the capacity to generate crest-derived autonomic neurons in early embryonic life (Ayer-Le Lievre and Le Douarin, 1982; Le Douarin, 1986; Fontaine-Perus et al., 1988; Douarin et al., 1991). Given that Phox2b is necessary for the development and survival of autonomic neurons (Pattyn et al., 1999), we first asked whether nodose neural crest progenitors express Phox2b during development. We used immunohistology to examine the expression of Sox10 and Phox2b, two transcription factors that respectively mark glial cells and neurons in the nodose ganglion between E10.5 and E12.5 (Fig. 1A). At E10.5–E11.5, most Phox2b+ neurons have delaminated from the epibranchial placode and begun to coalesce in the nodose ganglia alongside Sox10+ glial cells derived from the neural crest and from nerve-associated crest progenitors (Fode et al., 1998; Zou et al., 2004). We found that ∼5% of Sox10+ cells in the nodose anlage coexpressed Phox2b between E10.5 and E12.5. The presence of Sox10+Phox2b+ cells was no longer observed by P4 (quantified in Fig. 1B). To exclude that these early Sox10+Phox2b+ cells represent an immature state of nodose neurons, we costained nodose ganglia with antibodies against Sox10 and the early postmitotic neuron marker Tlx3 at E11.5 and E12.5 (Kondo et al., 2008). This revealed that Sox10+ cells coexpressing Tlx3 were extremely rare (1/1,911 cells at E11.5, $n = 3$; 1/3,047 cells at E12.5, $n = 3$), suggesting that Sox10+ cells are not immature neurons. Thus, cells coexpressing Sox10 and Phox2b during early nodose ganglia development correspond to glial cells or nerve-associated crest progenitors.

To better visualize all cells with a history of Phox2b expression, we designed a lineage-tracing experiment where we crossed a $Phox2b^{Cre}$ mouse line with the reporter allele $R26^{nGFP}$ that expresses nuclear GFP upon Cre-mediated recombination and performed immunohistology against Phox2b and GFP. Phox2b begins to be expressed at E9.5 in migrating ectodermal neuroblasts as they begin to coalesce at the site of nodose ganglia formation and is maintained throughout life in nodose neurons (Pattyn et al., 1997; Fode et al., 1998; Lowenstein et al., 2023). The $Phox2b^{Cre}$ mouse line was generated by D'Autréaux et al. (2011) and faithfully recapitulates Phox2b expression when crossed with a fluorescence reporter (D'Autréaux et al., 2011). The resulting $Phox2b^{Cre};R26^{nGFP}$ mice were analyzed at E11.5 (Fig. 1C). We observed many GFP+Phox2b− cells along the vagus nerve (outlined with a dotted white line in Fig. 1C), suggesting that a subset of neural crest-derived cells transiently express Phox2b (i.e., expressed Phox2b prior to E11.5 and are thus GFP+ but already downregulated Phox2b expression and are Phox2b−) on their way to the nodose ganglion or other autonomic or enteric ganglia (Movie 1).

Recent research indicated that nerve-associated crest cells, also known as Schwann cell precursors, generate neurons and glial cells in parasympathetic ganglia (Dyachuk et al., 2014; Espinosa-Medina et al., 2014). In particular, starting at E10.5, all neural crest cells begin to associate themselves with peripheral nerves or ganglia, and by E11.5, they are bona fide Schwann cell precursors defined by their expression of $Sox8$, a recently described marker for late migrating crest cells/Schwann cell precursors that begin to attach to peripheral nerves at E11.5 (Adameyko et al., 2012; Dyachuk et al., 2014; Espinosa-Medina et al., 2014; Furlan et al., 2017; Kastriti et al., 2022). To clarify whether the Sox10+Phox2b+ cells described above correspond to Schwann cell precursors, we performed smFISH at E11.5 using probes against $Sox10$, $Phox2b$, and $Sox8$ mRNA (Fig. 1D). This revealed that many $Sox10+Phox2b+$ cells were also positive for the Schwann cell precursor marker $Sox8$ (Fig. 1D, white circles). The fact that (1) many GFP+Phox2b− cells in $Phox2b^{Cre};R26^{nGFP}$ mice were found along the vagus nerve together with (2) our in situ data showing that many $Sox10+Phox2b+$ cells also coexpress $Sox8$ suggests that they are Schwann cell precursors. A schema
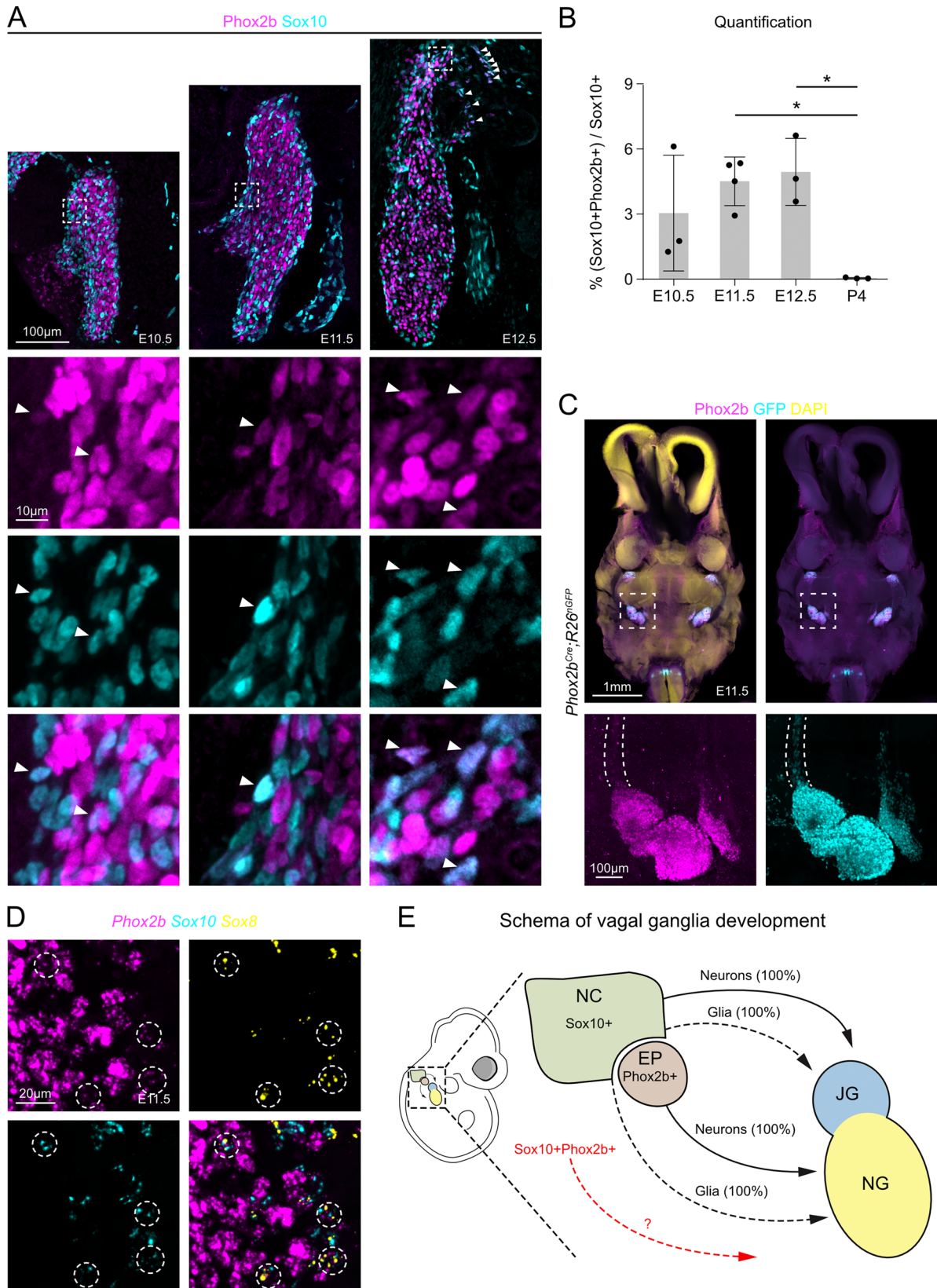
Figure 1. Some Sox10+ cells in the nodose anlage transiently express Phox2b during early development. **A**, Immunohistology of sagittal sections of the nodose anlage at E10.5, E11.5, and E12.5 using antibodies against Phox2b (magenta) and Sox10 (cyan). Magnifications of the boxed regions are shown below. Arrows mark Sox10+Phox2b+ cells. **B**, Quantifications revealed that $3.0 \pm 2.7\%$, $4.5 \pm 1.1\%$, and $4.9 \pm 1.5\%$ of Sox10+ cells in the nodose ganglia coexpress Phox2b at E10.5, E11.5, and E12.5, respectively. Shortly after birth at P4, $0.0 \pm 0.0\%$ of Sox10+ cells express Phox2b, and these proteins are exclusively present in nodose glial cells and neurons, respectively. $N = 3$–4. **C**, Immunohistology of a CUBIC cleared 300 μm transverse section from an E11.5 $Phox2b^{Cre};R26^{nGFP}$ embryo using antibodies against Phox2b (magenta) and GFP (cyan). DAPI was used as a counterstain (yellow). One nodose ganglion is shown magnified below, and the vagus nerve is outlined with dotted lines. Note that there are many GFP+Phox2b− cells along the nerve. **D**, smFISH (RNAscope) against $Phox2b$ (magenta), $Sox10$ (cyan), and $Sox8$ (yellow) mRNA. White dotted circles show $Phox2b+Sox10+Sox8+$ cells. **E**, A schema showing vagal ganglia development. The neural crest (NC, olive green) contains Sox10+ progenitors that give rise to

Phox2b GFP
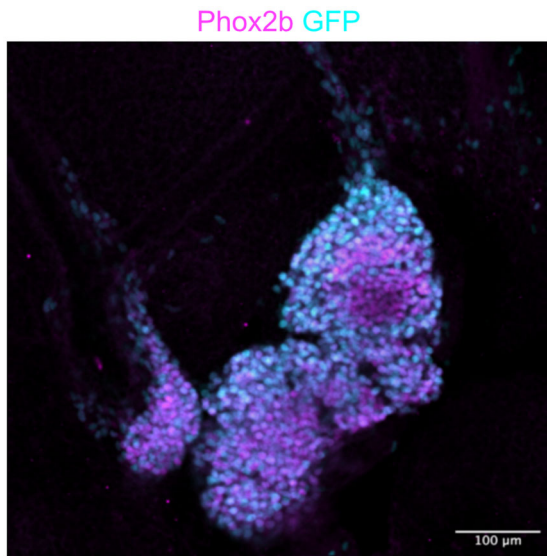
Movie 1. A z-stack of optical sections from an immunohistology experiment showing a CUBIC-cleared 300 μm transverse section from an E11.5 $Phox2b^{Cre};R26^{nGFP}$ vagal ganglion using antibodies against Phox2b (magenta) and GFP (cyan). [View online]

of vagal ganglia development is shown in Figure 1E, and the Sox10+Phox2b+ cells described here are highlighted in red.

A large proportion of nodose glial cells derived from the neural crest have a history of Phox2b expression

To identify all nodose glial cells with a history of Phox2b expression, we carried out a long-term lineage–tracing experiment using $Phox2b^{Cre};R26^{nGFP}$ animals and performed immunofluorescence at P4 (see Fig. 2A for a schematic display of the genetic strategy). Nodose ganglia were identified by their expression of Phox2b and distinguished from the neighboring Phox2b− jugular ganglia by the latter's expression of TrkA (Fig. 2B; Nassenstein et al., 2010; Kupari et al., 2019). We found that in the nodose ganglia of $Phox2b^{Cre};R26^{nGFP}$ mice, almost all Phox2b+ cells expressed GFP (97.3 ± 2.8%; $n = 3$), but surprisingly only half (44.1 ± 11.1%, $n = 3$) of GFP+ cells coexpressed Phox2b (Fig. 2C, left). Next, we stained the nodose ganglia with antibodies against Sox10 and Tlx3 to determine the identity of GFP+Phox2b− cells in $Phox2b^{Cre};R26^{nGFP}$ animals. This indicated that a large proportion (50.4 ± 8.3%; $n = 3$) of GFP+ cells in the nodose ganglia expressed Sox10, whereas the remainder (53.4 ± 6.8%; $n = 4$) expressed Tlx3 (Fig. 2C, middle and right). Lastly, we also determined the proportion of Sox10+ cells that coexpressed GFP and found that roughly 35.2 ± 2.3% ($n = 3$) of all nodose glial cells have a history of Phox2b expression (Fig. 2C, middle). Thus, many nodose glial cells transiently expressed Phox2b during their development.

We next asked whether the Sox10+ cells with a history of Phox2b expression in the nodose ganglia belong to a lineage distinct from the Wnt1+ neural crest lineage. For this, we performed a second lineage-tracing experiment using the $Wnt1^{Cre}$ mouse line together with the $R26^{nGFP}$ reporter (Fig. 2A). Wnt1

is expressed early during neural development at the dorsal midline of the neural tube in the premigratory neural crest (Gavin et al., 1990; Dorsky et al., 1998; Wu et al., 2003; Soldatov et al., 2019). The $Wnt1^{Cre}$ mouse line was generated by Danielian et al. (1998) and when crossed to a fluorescent reporter line labels all neural crest derivatives (Danielian et al., 1998; Soldatov et al., 2019; Kastriti et al., 2022). Thus, although Wnt1 is expressed only transiently and much earlier during development than Phox2b, $Wnt1^{Cre}$ is a great tool to label all neural crest derivatives, while $Phox2b^{Cre}$ labels all cells with a history of Phox2b expression. The proportion of Phox2b+ and Sox10+ cells deriving from Wnt1+ neural crest progenitors was determined at P4. Analysis of $Wnt1^{Cre};R26^{nGFP}$ mice revealed that GFP was expressed in 99 ± 0.7% ($n = 3$) of Sox10+ glial cells in the nodose ganglion, compared with only 2.4 ± 3.0% ($n = 3$) of Phox2b+ neurons (Fig. 2D). This result confirms previous data showing that all glial, but not neuronal, cells in the nodose ganglia are neural crest-derived and thus the Sox10+Phox2b+ cells belong to the neural crest, and not placodal, lineage.

To assess whether our $Phox2b^{Cre}$ mouse line was aberrantly active in neural crest derivatives and incorrectly labeled 35.2 ± 2.3% of Sox10+ nodose glial cells (Fig. 2C, middle), we compared the contributions made by the neural crest and epibranchial placodes to the neuronal populations of the jugular and nodose ganglia. To this end, we carried out long-term lineage–tracing experiments using either $Wnt1^{Cre}$ or $Phox2b^{Cre}$ in combination with the reporter allele Tau^{nLacZ} that expresses nuclear β-galactosidase (β-gal) protein exclusively in postmitotic neurons following Cre-mediated recombination and performed immunofluorescence at P4 (see Fig. 2E for a schematic display of the genetic strategy). We first analyzed β-gal+ cells in the jugular and nodose ganglia of $Wnt1^{Cre};Tau^{nLacZ}$ and $Phox2b^{Cre};Tau^{nLacZ}$ mice and observed that the vast majority of β-gal+ cells coexpressed Tlx3 (Fig. 2F, left; 95.7 ± 2.6%; $n = 3$; Fig. 3G, left; 99.6 ± 0.4%; $n = 3$), thus confirming that our genetic strategy specifically labeled neuronal derivatives. In the jugular ganglion, 81.8 ± 5.1% of β-gal+ neurons coexpressed TrkA in $Wnt1^{Cre};Tau^{nLacZ}$ mice (Fig. 2F, right; $n = 3$), whereas virtually all nodose neurons expressed TrkB in $Phox2b^{Cre};Tau^{nLacZ}$ animals (Fig. 2G, right; 99.0 ± 1.4%; $n = 3$). These experiments demonstrated that, as expected, TrkA+ jugular neurons derive from the Wnt1+ neural crest, while TrkB+ nodose neurons arise from placodally derived Phox2b+ neuroblasts. Taken together, we conclude that two distinct neural crest Wnt1+ lineages contribute to vagal ganglion derivatives: (1) a Wnt1+Phox2b− population that differentiates into neurons and glial cells of the jugular ganglia, as well as to roughly 60% of nodose glial cells, and (2) a Wnt1+Phox2b+ population that selectively generates roughly 40% of nodose glial cells.

To better examine the contribution of Wnt1+Phox2b+ progenitors to the nodose ganglia, we designed an intersectional genetic lineage-tracing strategy to mark all cells with a history of Wnt1 and Phox2b expression. We generated $Wnt1^{Cre};Phox2b^{FlpO}$ double transgenic animals and crossed them together with the reporter $R26^{ds-nGFP}$ line that expresses nuclear GFP after Cre- and Flp-mediated recombination (see Fig. 3A for a

←

neurons (solid lines) and glial cells (dotted lines) of the jugular ganglia (JG, blue) and glia of the nodose ganglia (NG, yellow). NG neurons derive from the Phox2b+ epibranchial placode (EP, beige). The derivatives from Sox10+Phox2b+ cells are unknown and are shown in red. Data are represented as mean ± SD; *$p < 0.05$; ordinary one-way ANOVA with Tukey's multiple-comparison test (**B**). Abbreviations: JG, jugular ganglia; NG, nodose ganglia; NC, neural crest; EP, epibranchial placode.
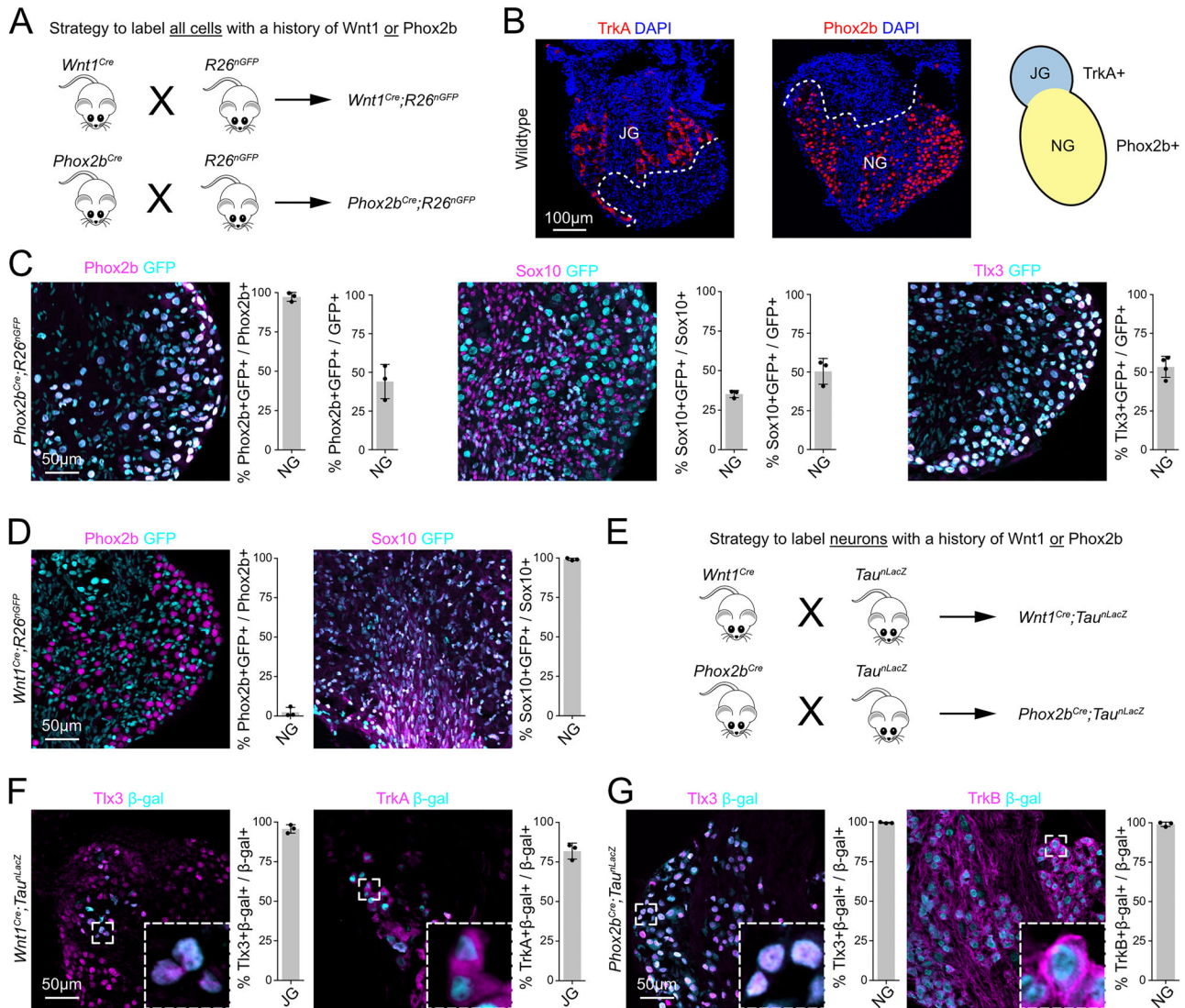
Figure 2. Nodose glial cells have a history of Phox2b expression. ***A***, A schema outlining the genetic lineage-tracing strategy used to label all cells with a history of either Wnt1 or Phox2b. We crossed *Wnt1^{Cre}* or *Phox2b^{Cre}* animals with *R26^{nGFP}* reporter mice to generate *Wnt1^{Cre};R26^{nGFP}* and *Phox2b^{Cre};R26^{nGFP}* mice. In these animals, all cells that expressed or express Wnt1 (in *Wnt1^{Cre}; R26^{nGFP}*) or Phox2b (in *Phox2b^{Cre};R26^{nGFP}*) will express a nuclear GFP. ***B***, We used immunohistology against TrkA (red) and Phox2b (red) to distinguish between the neighboring TrkA+Phox2b− jugular ganglion (JG) and the TrkA-Phox2b+ nodose ganglion (NG). Dotted white lines show the boundary between the jugular and nodose ganglia. For clarity a vagal ganglion is shown schematically on the right. ***C***, Immunohistology experiments in the nodose ganglia of *Phox2b^{Cre};R26^{nGFP}* mice at P4. Immunohistology against GFP (cyan) and Phox2b (magenta, left); quantifications show that 97.3 ± 2.8% of Phox2b+ cells are GFP+, but surprisingly only 44.1 ± 11.1% of GFP+ cells are Phox2b+; $n = 3$. Immunohistology against GFP (cyan) and Sox10 (magenta, middle), quantifications show that unexpectedly 35.2 ± 2.3% of Sox10+ cells are GFP+, and 50.4 ± 8.3% of GFP+ cells are Sox10+; $n = 3$. Immunohistology against GFP (cyan) and Tlx3 (magenta, right); quantification shows that 53.4 ± 6.8% of Tlx3+ cells are GFP+; $n = 4$. ***D***, Immunohistology experiments in the nodose ganglia of *Wnt1^{Cre};R26^{nGFP}* mice at P4. Immunohistology against GFP (cyan) and Phox2b (magenta, left); quantifications show that 2.4 ± 3.0% of Phox2b+ cells are GFP+; $n = 3$. Immunohistology against GFP (cyan) and Sox10 (magenta, middle); quantifications show that 99.1 ± 0.7% of Sox10+ cells are GFP+; $n = 3$. ***E***, A schema outlining the genetic lineage-tracing strategy used to label neurons with a history of either Wnt1 or Phox2b. We crossed *Wnt1^{Cre}* or *Phox2b^{Cre}* animals with *Tau^{nLacZ}* reporter mice to generate *Wnt1^{Cre};Tau^{nLacZ}* and *Phox2b^{Cre};Tau^{nLacZ}* mice. In these animals, neurons that expressed or express Wnt1 (in *Wnt1^{Cre};Tau^{nLacZ}*) or Phox2b (in *Phox2b^{Cre};Tau^{nLacZ}*) will express a nuclear β-galactosidase. ***F***, Immunohistology experiments in the jugular ganglia of *Wnt1^{Cre}; Tau^{nLacZ}* mice at P4. Immunohistology against β-gal (cyan) and Tlx3 (magenta, left); quantification shows that 95.7 ± 2.6% of β-gal+ cells are Tlx3+; $n = 3$. Immunohistology against β-gal (cyan) and TrkA (magenta, left); quantification shows that 81.8 ± 5.0% of β-gal+ cells are TrkA+; $n = 3$. Magnifications of the boxed regions are shown in the inset. ***G***, Immunohistology experiments in the nodose ganglia of *Phox2b^{Cre};Tau^{nLacZ}* mice at P4. Immunohistology against β-gal (cyan) and Tlx3 (magenta, left); quantification shows that 99.6 ± 0.4% of β-gal+ cells are Tlx3+; $n = 3$. Immunohistology against β-gal (cyan) and TrkB (magenta, left); quantification shows that 99.0 ± 1.4% of β-gal+ cells are TrkB+; $n = 3$. Magnifications of the boxed regions are shown in the inset.

schematic display of the genetic strategy). Vagal ganglia from *Wnt1^{Cre};Phox2b^{FlpO};R26^{ds-nGFP}* mice were analyzed at P4 using immunohistology. We first examined whether any TrkA+ jugular or Phox2b+ nodose neurons were GFP+ and found that GFP+ cells rarely expressed either of these neuronal markers (Fig. 3B; $n = 3$). In the nodose ganglia, 96.9 ± 0.7% of GFP+ cells coexpressed Sox10, and 38.4 ± 2.6% of Sox10+ cells expressed GFP

(Fig. 3C; $n = 3$). Furthermore, the overwhelming majority of GFP+ cells (96.4 ± 2.1%) were located in the nodose ganglia, while the remaining GFP+ cells (3.8 ± 2.3%) were located in the TrkA+ jugular ganglia (Fig. 3C; $n = 3$). We conclude that roughly 40% of Sox10+ glial cells in the nodose ganglia derive from a neural crest progenitor population that transiently expresses Phox2b (summarized in Fig. 3F). Thus, by virtue of (1) their
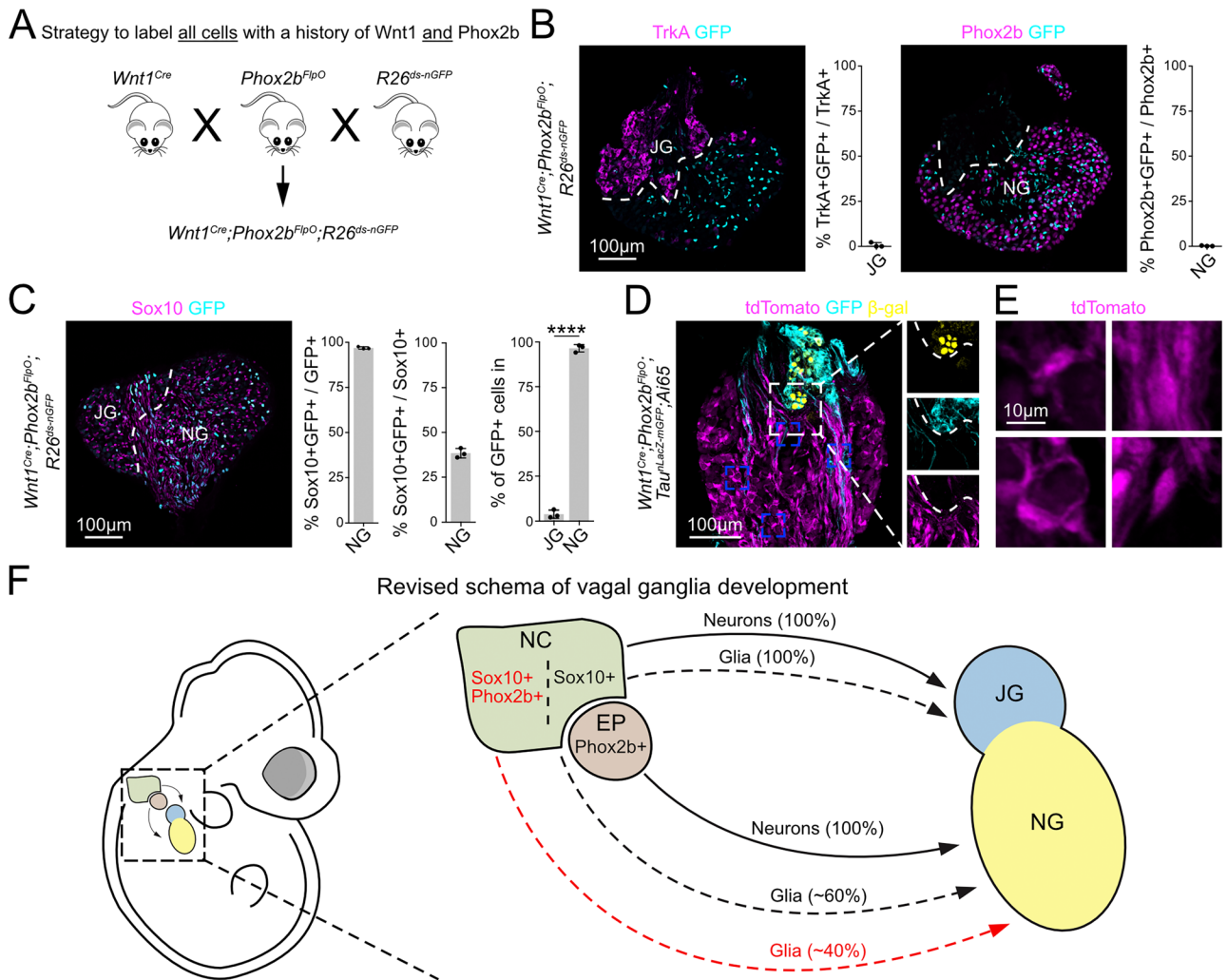
Figure 3. Nodose glial cells with a history of Phox2b expression are crest-derived. **A**, To specifically label the progeny from all cells that have a history of both Wnt1 and Phox2b expression, we used a reporter mouse that expresses nuclear GFP from the Rosa locus only after Cre- and Flp-mediated stop cassette excision ($R26^{ds-nGFP}$) together with $Wnt1^{Cre}$ and $Phox2b^{FlpO}$. **B**, We examined the vagal ganglia from $Wnt1^{Cre};Phox2b^{FlpO};R26^{ds-nGFP}$ animals at P4 and performed immunohistology against GFP (cyan), together with TrkA (magenta, left) and Phox2b (magenta, right). Almost no TrkA+ jugular neurons ($0.8 \pm 1.3\%$, $n = 3$) or Phox2b+ nodose neurons ($0.2 \pm 0.2\%$, $n = 3$) were GFP+. **C**, Immunohistology against GFP (cyan) and Sox10 (magenta) in $Wnt1^{Cre};Phox2b^{FlpO};R26^{ds-nGFP}$ at P4 revealed that $96.9 \pm 0.7\%$ of all GFP+ cells were Sox10+ and $38.4 \pm 2.6\%$ of all nodose Sox10+ cells were GFP+; $n = 3$. GFP+ cells were located in the nodose rather than the jugular ganglia ($96.4 \pm 2.1\%$ vs $3.8 \pm 2.2\%$; $p < 0.0001$; $n = 3$). **D**, $Wnt1^{Cre};Phox2b^{FlpO}$ animals were crossed together with a reporter mouse harboring (1) the Ai65 allele that will express cytoplasmic tdTomato from the Rosa locus only after Cre- and Flp-mediated stop cassette excision in all cells and (2) the $Tau^{nLacZ-mGFP}$ allele that will express a nuclear β-galactosidase and membrane GFP from the Tau locus after Cre-mediated stop cassette excision specifically in neurons. We examined the vagal ganglia from $Wnt1^{Cre};Phox2b^{FlpO};Tau^{nLacZ-mGFP};Ai65$ animals at P4 and performed immunohistology against GFP (cyan), together with tdTomato (magenta) and β-gal (yellow). The dotted white box is shown magnified to the right. **E**, Magnifications of individual tdTomato+ glial cells (magenta) from dotted blue boxes in **D**. **F**, A schema showing vagal ganglia development. The neural crest (NC, olive green) contains Sox10+ progenitors that give rise to neurons (solid lines) and glial cells (dotted lines) of the jugular ganglia (JG, blue) and the newly described Sox10+Phox2b+ progenitors that give rise to glia (dotted red line) of the nodose ganglia (NG, yellow). NG neurons derive from the Phox2b+ epibranchial placode (EP, beige). Data are represented as mean ± SD; ****$p < 0.0001$; unpaired two-tailed t test (J). Abbreviations: JG, jugular ganglia; NG, nodose ganglia; NC, neural crest; EP, epibranchial placode.

spatial localization to the nodose, but not jugular, ganglia and (2) transient expression of Phox2b, these progenitors seem to represent the same population of bipotent crest-derived cells that were first described by Le Douarin to have the potential to generate autonomic or enteric, but not somatosensory, neurons.

Lastly, in an orthogonal approach, we used a similar intersectional genetic lineage-tracing strategy as above with $Wnt1^{Cre};Phox2b^{FlpO}$ double transgenic animals but instead crossed them with $Tau^{nLacZ-mGFP};Ai65$ mice to generate $Wnt1^{Cre};Phox2b^{FlpO};Tau^{nLacZ-mGFP};Ai65$ animals. These mice will express nuclear β-galactosidase and membrane GFP after Cre-mediated recombination in all neurons that derive from the Wnt1+ neural crest

(i.e., jugular neurons) and cytoplasmic tdTomato in all neural crest cells with a history of Phox2b expression (i.e., nodose glial cells) after Cre- and Flp-mediated recombination (Fig. 3D). This genetic approach shows how the crest-derived glial cells with a history of Phox2b (labeled by tdTomato) selectively populate the nodose ganglia and avoid the jugular ganglia (demarcated with GFP and β-gal).

As this genetic strategy labeled the entire cytoplasm of crest-derived cells with a history of Phox2b with fluorescent tdTomato protein, the morphology of these glial cells could be examined. Magnifications (dotted blue boxes) show various distinct morphologies, including cells that are ramified (Fig. 3E, top left), elongated along an axonal tract (Fig. 3E, top right), wrapping

nodose soma (Fig. 3E, bottom left), and compact (Fig. 3E, bottom right), thus suggesting that the crest-derived progenitors with a history of Phox2b generate numerous distinct glial cell types in the nodose ganglia.

scRNA-seq reveals that nodose glial cells with a history of Phox2b contribute to all major glial cell subtypes in the nodose ganglia

Our data from early embryonic development indicated that a proportion of Sox10+ cells located along the vagus nerve and in the nodose anlage transiently express Phox2b between E10.5 and E12.5 (Fig. 1). Previous work demonstrated that Sox10+Phox2b+ parasympathetic nerve-associated crest progenitors generate Schwann cells (Dyachuk et al., 2014; Espinosa-Medina et al., 2014), although it is unknown whether such progenitors can give rise to other glial cell types. To investigate which postnatal glial cell types are generated from Sox10+Phox2b+ progenitors, we used Phox2b^{Cre};Ai14 mice to drive the expression of tdTomato fluorescent protein in all cells with a history of Phox2b expression. This strategy permanently labeled all derivatives from (1) the epibranchial placode (nodose neurons displaying sustained Phox2b expression) and (2) Sox10+Phox2b+ crest-derived cells (glial cells displaying transient Phox2b expression) with cytoplasmic tdTomato protein (Fig. 4A). We dissected the vagal ganglia from Phox2b^{Cre};Ai14 mice at P4 and dissociated them into a single-cell suspension using a neuronal depletion protocol to focus our downstream analyses on non-neuronal cells with a history of Phox2b expression (Fig. 4A; see Materials and Methods). Next, we used flow cytometry to sort 384 tdTomato+ cells and generated libraries for next-generation sequencing using the low-throughput, high-sensitivity CEL-Seq2 method (Fig. 4A; Hashimshony et al., 2016). After sequencing, 291 (76%) cells passed quality control (see Materials and Methods). We detected a median of 4,484 genes and 11,900 unique molecular identifiers (UMIs) per cell (Fig. 4B).

Further analysis distinguished four glial cell subtypes: NMSCs (135 cells, 46% of total), SG (82 cells, 28% of total), MSCs (37 cells, 13% of total), and GPs (37 cells, 13% of total; Fig. 4C). The four glial subtypes were identified using differential expression of known marker genes (described below). Thus, the Sox10+Phox2b+ neural crest-derived glial progenitors give rise to all major glial cell subtypes in the nodose ganglia.

We identified subtype-specific marker genes by performing differential gene expression analysis for each subtype (Tables 1 and 2). The top five marker genes per subtype ranked by average log fold change are displayed in a heatmap, and the genes used for further characterization are shown in red (Fig. 4D). Violin plots for the subtype markers are shown in Figure 4E. All cells expressed high levels of pan-glial markers Apoe and Sox10, confirming that our approach specifically purified glial cells (Fig. 4F; Boyles et al., 1985; Kuhlbrodt et al., 1998; Britsch et al., 2001; Duan et al., 2007; Zhou et al., 2019).

NMSCs made up the largest group of cells (46% of all cells) and were defined by their expression of Scn7a (Nav2.1 or Na$_x$), Ngfr (P75), and L1cam (Fig. 4G; Table 1; Watanabe et al., 2002; Wolbert et al., 2020; Tasdemir-Yilmaz et al., 2021). Gene ontology (GO) term analysis revealed that the NMSC subtype was enriched for the terms "extracellular matrix organization," "blood vessel morphogenesis," and "extracellular structure organization," suggesting that they provide structural support to nodose neurons (Fig. 5).

SG, comprising 28% of the sequenced cells, expressed known SG markers such as Fabp7 (BLBP or BFABP), Adamts5, and Ctnnd2 (Fig. 4G; Table 1; Kurtz et al., 1994; Avraham et al., 2020, 2022; Tasdemir-Yilmaz et al., 2021). GO term analysis for enriched biological processes revealed "extracellular matrix organization," "cell-substrate adhesion," and terms related to metabolism such as "sterol biosynthetic process" (Fig. 5). Thus, SG seem to be the peripheral equivalent of astrocytes, a central nervous system glial cell type that performs a homeostatic role in the brain (Hanani and Verkhratsky, 2021).

MSCs, forming 13% of all cells, expressed well-characterized marker genes such as Pou3f1 (Oct6), Prx (Periaxin), and Mag (Myelin-associated glycoprotein; Fig. 4G; Table 1; Bermingham et al., 1996; Jaegle et al., 1996). GO term analysis revealed terms such as "axon ensheathment," "ensheathment of neurons," and "myelination" (Fig. 5).

GPs comprised 13% of all cells and were enriched for genes typically expressed in proliferating cells such as MKi67 (Marker of Proliferation Ki-67), Top2a (DNA Topoisomerase II Alpha), Cenpe, and Cenpf (Centromere Protein E and F; Fig. 4G; Table 1). Lastly, GO term analysis confirmed that these cells are highly proliferative as the top enriched terms were "chromosome segregation," "nuclear division," and "organelle fission" (Fig. 5).

In summary, our bioinformatics analyses revealed that all glial cell types, including Schwann cells, SG, and GPs, derive from Sox10+Phox2b+ neural crest progenitors (Fig. 4). We further identified marker genes for each subtype, NMSC (Scn7a), SG (Fabp7), MSC (Pou3f1), and GP (MKi67), and GO term analysis revealed their putative functions. Lastly, we employed hierarchical clustering to examine the relationships between glial subtypes (Fig. 4H). We found that GP and MSC are the most transcriptomically unique cell types, while NMSC and SG are the most similar to one another. This reflects their biology as GP and MSC have specialized roles in proliferation and myelination, respectively, while NMSCs and SG have overlapping functional roles as both provide metabolic and structural support to neurons (Harty and Monk, 2017; Hanani and Spray, 2020; Hanani and Verkhratsky, 2021).

In vivo characterization of Phox2b derived glial cell subtypes in the nodose ganglia

Our scRNA-seq analysis (Fig. 4) showed that the four subtypes of nodose glial cells derive from Sox10+Phox2b+ neural crest progenitors. To confirm this in vivo, we performed smFISH on vagal ganglia sections from Phox2b^{Cre};R26^{nGFP} mice at P4 (Fig. 6). First, we confirmed that glial cells in the nodose ganglion have a history of Phox2b expression by combining immunohistology against GFP (green) together with smFISH to detect Sox10 and Phox2b mRNA (Fig. 6A, red). This revealed that many GFP+ cells with a history of Phox2b are glial cells as they express Sox10, but not Phox2b, mRNA (Fig. 6A, arrowheads). Next, we used immunohistology against GFP (green) together with smFISH probes against our four glial subtype markers (red): Scn7a to label NMSC, Fabp7 to label SG, Pou3f1 to label MSC, and MKi67 to label GP (Fig. 6B). Double positive cells that were GFP+Marker+ demonstrate that all four glial subtypes derive from progenitors with a history of Phox2b expression (Fig. 6B, arrowheads). We additionally tested whether there was any overlap between the glial subtypes in vivo using dual smFISH. Simultaneous expression of two subtype markers was exceedingly rare (Fig. 6C, arrowheads). Note that we could not test for overlap between Scn7a and Fabp7, as these probes were
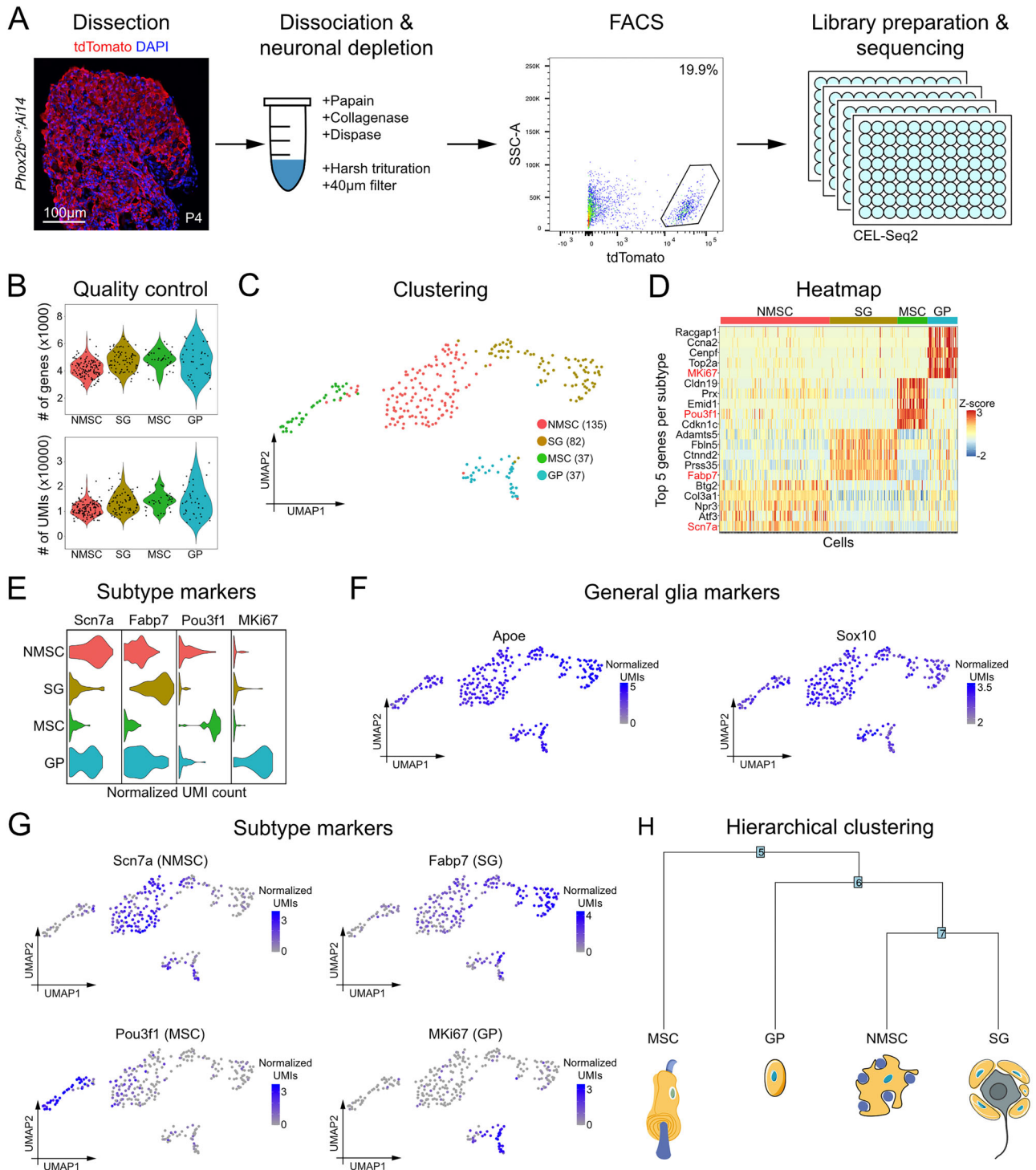
Figure 4. Bioinformatics analysis reveals that Sox10+Phox2b+ cells give rise to all major glial cell types in the nodose ganglia. *A*, In order to examine the derivatives from Sox10+Phox2b+ cells, we used *Phox2b^Cre* to drive the expression of a cytoplasmic tomato protein upon Cre-mediated excision of a stop cassette. Immunofluorescence at P4 showed many tdTomato+ cells in the nodose ganglion. To investigate the non-neuronal derivatives from Sox10+Phox2b+ cells, we dissociated the vagal ganglia from *Phox2b^Cre;Ai14* mice at P4 and employed a neuronal depletion protocol. After enzymatic digestion at 37℃, ganglia were harshly mechanically triturated and passed twice through a 40 µm filter. 384 tdTomato+ cells were then sorted into four 96-well plates using flow cytometry. scRNA-seq libraries were prepared using the CEL-Seq2 protocol and sequenced. *B*, We detected a median of 4,484 genes and 11,900 UMIs per cell. *C*, UMAP plot of non-neuronal Phox2b derivatives, with each subtype labeled in a different color. The UMAP plot revealed four transcriptomically unique non-neuronal subtypes: NMSCs (peach), SG (gold), MSCs (green), and GPs (blue). *D*, Heatmap showing the top five subtype-specific genes for each subtype, ranked by *p* value. Note the color code on top of the heatmap. The marker gene used to identify each subtype is shown in red. *E*, Violin plots showing the subtype markers. *Scn7a* labels NMSC, *Fabp7* labels SG, *Pou3f1* labels MSC, and *MKi67* labels GP. *F*, UMAP plots for general glia markers *Apoe* and *Sox10* showing that all cells in our analysis are glia. *G*, UMAP plots for each subtype marker. *H*, Hierarchical clustering dendrogram reveals that NMSC and SG are the most transcriptomically similar subtypes, while MSC and GP are different from each other and also from NMSC and SG. Illustrations were adapted from bioicons.com and scidraw.io and licensed under CC-BY 3.0 and CC-BY 4.0.

Table 1. Top 25 positive marker genes for each subtype ranked by average log fold change

Subtype	Gene	p_val	avg_log2FC	pct.1	pct.2	p_val_adj
NMSC	Scn7a	2.293350×10^{-21}	1.8096400	0.896	0.526	3.403790×10^{-17}
NMSC	Atf3	1.741530×10^{-10}	1.6949400	0.689	0.442	2.584780×10^{-06}
NMSC	Npr3	4.57638×10^{-20}	1.4968900	0.919	0.660	6.792260×10^{-16}
NMSC	Col3a1	1.292400×10^{-24}	1.1968700	1.000	1.000	1.918180×10^{-20}
NMSC	Btg2	1.591010×10^{-14}	1.1854300	0.800	0.442	2.36138×10^{-10}
NMSC	Ngfr	1.97471×10^{-14}	1.1628100	0.874	0.615	2.930860×10^{-10}
NMSC	Col1a1	1.666920×10^{-15}	1.1088000	0.993	0.897	2.474050×10^{-11}
NMSC	Cldn11	5.173700×10^{-14}	1.0777800	0.852	0.558	7.678810×10^{-10}
NMSC	Junb	3.941840×10^{-15}	1.0759200	0.963	0.769	5.850480×10^{-11}
NMSC	Wwp1	4.080780×10^{-19}	1.0731700	0.963	0.808	6.056690×10^{-15}
NMSC	Sbspon	5.809910×10^{-20}	1.0590800	0.904	0.526	8.623060×10^{-16}
NMSC	Zfp36	2.770460×10^{-11}	1.0588500	0.770	0.506	4.111910×10^{-07}
NMSC	Pcdh9	2.365680×10^{-16}	1.0567900	0.889	0.699	3.511140×10^{-12}
NMSC	Klf6	5.458960×10^{-14}	1.0414700	0.993	0.942	8.102180×10^{-10}
NMSC	Jun	6.714920×10^{-18}	1.0355400	1.000	0.987	9.96629×10^{-14}
NMSC	Ank3	4.258040×10^{-18}	1.0257900	0.963	0.750	6.319780×10^{-14}
NMSC	Socs3	6.653750×10^{-10}	0.9906640	0.933	0.756	9.875500×10^{-06}
NMSC	Adam23	2.600430×10^{-21}	0.9681050	0.970	0.712	3.85956×10^{-17}
NMSC	Mmp2	1.867270×10^{-11}	0.9630820	0.541	0.231	2.771410×10^{-07}
NMSC	Fosb	2.390370×10^{-11}	0.9559280	0.919	0.756	3.547780×10^{-07}
NMSC	Nrp2	2.292890×10^{-19}	0.9516040	0.985	0.910	3.403110×10^{-15}
NMSC	L1cam	8.473610×10^{-18}	0.9410370	0.985	0.795	1.257650×10^{-13}
NMSC	Egr1	1.873710×10^{-22}	0.9353060	0.985	0.974	2.780960×10^{-18}
NMSC	Fos	7.43264×10^{-20}	0.8856660	1.000	0.994	1.103150×10^{-15}
NMSC	Itgb4	7.665240×10^{-17}	0.8603860	0.956	0.808	1.137670×10^{-12}
SG	Fabp7	1.625270×10^{-28}	2.5923300	1.000	0.746	2.412230×10^{-24}
SG	Prss35	1.031×10^{-31}	1.9852900	1.000	0.703	1.53021×10^{-27}
SG	Ctnnd2	1.965640×10^{-28}	1.9377600	0.902	0.325	2.91741×10^{-24}
SG	Fbln5	2.284160×10^{-22}	1.8017900	0.951	0.646	3.390150×10^{-18}
SG	Adamts5	4.85133×10^{-23}	1.7161000	0.988	0.880	7.200340×10^{-19}
SG	Epas1	1.504860×10^{-19}	1.6923600	0.683	0.191	2.233510×10^{-15}
SG	Sfrp5	6.611460×10^{-27}	1.6030700	1.000	0.842	9.812720×10^{-23}
SG	Hey2	1.58619×10^{-23}	1.5686000	0.793	0.278	2.354220×10^{-19}
SG	Igfbp4	7.066290×10^{-24}	1.4410600	0.976	0.656	1.048780×10^{-19}
SG	Fgfr1	2.898070×10^{-23}	1.3774300	0.963	0.871	4.301320×10^{-19}
SG	Hmgcs1	1.431010×10^{-14}	1.3540200	0.976	0.856	2.123910×10^{-10}
SG	Fbln2	7.83637×10^{-20}	1.3491100	1.000	0.981	1.163070×10^{-15}
SG	Ptprz1	1.748870×10^{-25}	1.3472500	1.000	0.866	2.595670×10^{-21}
SG	Mapre2	8.630980×10^{-26}	1.3420500	1.000	0.947	1.28101×10^{-21}
SG	Mest	2.365160×10^{-19}	1.3084500	0.841	0.368	3.510370×10^{-15}
SG	Fmo1	4.524900×10^{-26}	1.3075000	0.756	0.148	6.715860×10^{-22}
SG	Cst3	6.591510×10^{-19}	1.2987000	1.000	1.000	9.783120×10^{-15}
SG	Col26a1	1.974480×10^{-23}	1.2945200	0.976	0.598	2.930520×10^{-19}
SG	Kit	2.220420×10^{-19}	1.2905500	0.841	0.407	3.295550×10^{-15}
SG	Cdh11	3.694750×10^{-21}	1.2681400	0.988	0.871	5.483740×10^{-17}
SG	Me1	6.068030×10^{-22}	1.2506400	0.939	0.612	9.006180×10^{-18}
SG	Acsbg1	9.033020×10^{-21}	1.2437700	0.963	0.627	1.34068×10^{-16}
SG	Lect1	4.310230×10^{-17}	1.2003300	0.561	0.115	6.397240×10^{-13}
SG	Bcan	1.937560×10^{-18}	1.1847100	0.451	0.043	2.875730×10^{-14}
SG	Ptgfrn	5.77765×10^{-21}	1.1834600	0.963	0.703	8.575190×10^{-17}
MSC	Cdkn1c	9.726940×10^{-19}	3.487770	0.946	0.559	1.443670×10^{-14}
MSC	Pou3f1	1.780720×10^{-24}	3.458290	0.973	0.339	2.642940×10^{-20}
MSC	Emid1	4.862800×10^{-17}	2.767230	0.676	0.150	7.217360×10^{-13}
MSC	Prx	5.12595×10^{-17}	2.682530	1.000	0.602	7.607940×10^{-13}
MSC	Cldn19	6.038190×10^{-24}	2.587130	0.946	0.260	8.961870×10^{-20}
MSC	Csrp2	1.019890×10^{-28}	2.292840	0.946	0.177	1.513720×10^{-24}
MSC	Slc36a2	3.963220×10^{-22}	2.252760	0.486	0.024	5.882210×10^{-18}
MSC	Pllp	2.256650×10^{-19}	2.182500	0.892	0.303	3.349320×10^{-15}
MSC	Ncmap	3.96161×10^{-18}	2.155490	0.541	0.059	5.879820×10^{-14}
MSC	Bzw2	1.406840×10^{-20}	2.119170	1.000	0.661	2.088030×10^{-16}
MSC	Fxyd6	1.587450×10^{-05}	2.071460	0.730	0.543	2.356090×10^{-01}
MSC	Kcna1	1.049730×10^{-16}	2.051000	0.973	0.654	1.558010×10^{-12}
MSC	Dusp15	8.926770×10^{-24}	1.957240	0.730	0.098	1.324910×10^{-19}
MSC	Peli2	1.021210×10^{-18}	1.882120	1.000	0.547	1.515690×10^{-14}
MSC	Mag	5.228600×10^{-07}	1.837180	0.703	0.402	7.760300×10^{-03}

(Table continues.)

Table 1. Continued

Subtype	Gene	p_val	avg_log2FC	pct.1	pct.2	p_val_adj
MSC	Gldn	2.930020×10^{-27}	1.788630	0.514	0.012	4.34874×10^{-23}
MSC	Gypc	5.145070×10^{-30}	1.765670	0.946	0.157	7.636310×10^{-26}
MSC	Cuedc2	1.645480×10^{-12}	1.748400	0.973	0.909	2.442220×10^{-08}
MSC	Fa2h	6.295160×10^{-17}	1.670290	0.838	0.260	9.343270×10^{-13}
MSC	Nkd1	1.695490×10^{-17}	1.665320	0.865	0.295	2.516450×10^{-13}
MSC	Nav1	7.530500×10^{-16}	1.650030	1.000	0.587	1.117680×10^{-11}
MSC	Rasal2	3.190570×10^{-14}	1.649170	0.919	0.598	4.735440×10^{-10}
MSC	Mpp6	2.898890×10^{-14}	1.642210	0.757	0.260	4.302530×10^{-10}
MSC	Smtn	7.675250×10^{-16}	1.638570	0.946	0.575	1.139160×10^{-11}
MSC	Cdkn1a	4.588970×10^{-10}	1.615640	0.865	0.622	6.810940×10^{-06}
MSC	Cdkn1c	9.726940×10^{-19}	3.487770	0.946	0.559	1.443670×10^{-14}
GP	Mki67	2.213570×10^{-28}	3.294410	0.865	0.142	3.285380×10^{-24}
GP	Top2a	1.623500×10^{-13}	3.264510	0.703	0.240	2.409610×10^{-09}
GP	Cenpf	2.075460×10^{-33}	2.874150	0.946	0.142	3.080400×10^{-29}
GP	Ccna2	1.42824×10^{-19}	2.409520	0.595	0.075	2.119790×10^{-15}
GP	Racgap1	6.308420×10^{-18}	2.219260	0.676	0.138	9.362960×10^{-14}
GP	Cenpe	3.353500×10^{-31}	2.216910	0.784	0.071	4.977270×10^{-27}
GP	Prc1	8.622960×10^{-16}	2.212550	0.649	0.138	1.27982×10^{-11}
GP	Smc4	2.181510×10^{-14}	2.165200	0.892	0.539	3.2378×10^{-10}
GP	Cdca3	1.681540×10^{-29}	2.116250	0.784	0.079	2.495730×10^{-25}
GP	Ckap2	4.220610×10^{-22}	2.054730	0.730	0.118	6.264240×10^{-18}
GP	Ube2c	2.897680×10^{-18}	1.969250	0.514	0.051	4.300740×10^{-14}
GP	Tpx2	5.849750×10^{-19}	1.925130	0.676	0.122	8.682200×10^{-15}
GP	Ckap2l	7.525890×10^{-21}	1.907690	0.541	0.047	1.116990×10^{-16}
GP	Hmmr	2.053700×10^{-25}	1.902600	0.568	0.031	3.048090×10^{-21}
GP	Ncapd2	2.185970×10^{-14}	1.858290	0.703	0.220	3.244420×10^{-10}
GP	Ccnb1	6.07373×10^{-21}	1.814920	0.568	0.055	9.014630×10^{-17}
GP	Cenpa	3.704130×10^{-15}	1.814340	0.784	0.240	5.497670×10^{-11}
GP	Aspm	1.94084×10^{-24}	1.787550	0.676	0.071	2.880590×10^{-20}
GP	Fam64a	2.994340×10^{-32}	1.770000	0.649	0.024	4.444200×10^{-28}
GP	Rangap1	1.151960×10^{-12}	1.769080	0.811	0.445	1.709740×10^{-08}
GP	H2afx	6.125160×10^{-15}	1.767560	0.649	0.161	9.090970×10^{-11}
GP	Tubb4b	9.260160×10^{-10}	1.748440	0.919	0.736	1.374390×10^{-05}
GP	Cdk1	5.269720×10^{-12}	1.726110	0.514	0.110	7.821320×10^{-08}
GP	Ccnb2	4.120760×10^{-26}	1.714110	0.703	0.067	6.116030×10^{-22}
GP	Tubb6	3.836680×10^{-12}	1.667550	0.703	0.268	5.694410×10^{-08}

incompatible. Our bioinformatics analysis uncovered additional genes specifically expressed in each glial subtype (Fig. 6D). Our data show that all four glial subtypes that derive from Sox10+Phox2b+ neural crest progenitors are present in vivo in nodose ganglia at P4 (summarized in Fig. 6E).

Dataset integration of peripheral glial cells reveals transcriptomic similarities between DRG and nodose ganglia glial cells

In order to further explore the transcriptional heterogeneity of peripheral glial cells, we performed an integration analysis of our data of Sox10+Phox2b+ crest-derived nodose glial cells, combining our data with that of a recent scRNA-seq study that included developing and mature glia from the auditory cochlea spiral ganglia and the somatosensory DRG (Tasdemir-Yilmaz et al., 2021). This dataset was of particular interest because it contains cells from the spiral ganglia, which like the nodose ganglia contains both crest and placode derivatives, with its glial cells deriving from the neural crest and its support cells and neurons deriving from the otic placode (D'amico-Martel and Noden, 1983; Breuskin et al., 2010). Our dataset integration included 291 nodose glial cells with a history of Phox2b (this study, Fig. 7A, top) together with 7,695 cochlea cells and 21,612 glial cells from lumbar DRG and sciatic nerve (Fig. 7A, bottom; Tasdemir-Yilmaz et al., 2021). To integrate scRNA-seq data across developmental (from embryonic to postnatal stages) and biological (nodose and spiral ganglia and DRG) scales is a complicated undertaking due to batch effects and technical noise. Here, we performed dataset integration using the CCA approach as implemented in Seurat (Hao et al., 2021). UMAP analysis visually confirmed that the datasets were well integrated with one another by revealing that nodose glial cells (color-coded by subtype in Fig. 7B, top), and DRG/cochlea glial cells (color-coded by subtype in Fig. 7B, bottom) were mixed together.

Next we used Suerat's cell-type label transfer pipeline to identify which of the DRG/cochlea subtypes most closely correspond to our nodose glial subtypes (Hao et al., 2021). This approach is similar to integration but assigns subtype labels from the reference dataset (DRG/cochlea subtypes from Tasdemir-Yilmaz et al., 2021) to the cells of the query dataset (nodose glial subtypes). The dataset from Tasdemir-Yilmaz et al. (2021) had many more cells, therefore more subtypes and better resolution. Thus, we decided to map our data to theirs, transferring their subtype labels to our cells. The correlation between nodose glial and DRG/cochlea subtypes from the integration (displayed visually in the UMAPs in Fig. 7B) was recapitulated with an orthogonal approach, cell-type label transfer (displayed with a Sankey plot; Fig. 7C).

The latter approach revealed the correspondences between nodose glial subtypes and the DRG/cochlea subtypes: GPs to g4 and g5, with minor contributions to g1 and g6; SG cells to g1, g2, and g5; NMSCs to g5; and MSCs to g7, with smaller contributions to g5 and g6 (Fig. 7C).

Table 2. Resource list of all mouse lines, antibodies, and RNAscope probes used

Mouse lines

	Catalog #	RRID	Source	Reference
Ai14	#007914	IMSR_JAX:007914	The Jackson Laboratory	Madisen et al. (2010).
Ai65	#021875	IMSR_JAX:021875	The Jackson Laboratory	Madisen et al. (2015).
Tau^{nLacZ-mGFP}	N/A	IMSR_JAX:021162	Kindly provided by Silvia Arber	Hippenmeyer et al. (2005).
R26^{ds-nGFP}	N/A	N/A	Kindly provided by Martyn Goulding	Stam et al. (2012).
Wnt1^{Cre}	N/A	IMSR_JAX:3360	Kindly provided by Andrew McMahon	Danielian et al. (1998).
Phox2b^{Cre}	N/A	IMSR_JAX:07452	Kindly provided by Jean-François Brunet	D'Autréaux et al. (2011).
Phox2b^{FlpO}	N/A	IMSR_JAX:022407	Kindly provided by Jean-François Brunet	Hirsch et al. (2013).

Antibodies

	Catalog #	RRID	Source	Reference	Dilution	Species
α-GFP	GF090R	AB_2314545	Nacalai Tesque	N/A	1:1,000	Rat
α-GFP	GFP-1020	AB_10000240	Aves Labs	N/A	1:500	Chicken
α-RFP	orb334992	N/A	Biorbyt	N/A	1:500	Goat
α-RFP	600-401-379-RTU	AB_2209751	Rockland Immunochemicals	N/A	1:500	Rabbit
α-β-gal	ab134435	AB_2737437	Abcam	N/A	1:1,000	Chicken
α-Tlx3	N/A	N/A	Kindly provided by Thomas Müller	Müller et al. (2005).	1:5,000	Guinea pig
α-Phox2b	AF4940	AB_10889846	R&D Systems	N/A	1:200	Goat
α-Phox2b	N/A	N/A	Kindly provided by Jean-François Brunet	Pattyn et al. (1997)	1:500	Rabbit
α-Sox10	AF2864	AB_442208	R&D Systems	N/A	1:200	Goat
α-Sox10	ab227680	AB_2927464	Abcam	N/A	1:200	Rabbit
α-TrkA	AF175	AB_354970	R&D Systems	N/A	1:500	Goat
α-TrkB	AF1494	AB_2155264	R&D Systems	N/A	1:300	Goat

RNAscope probes

	Catalog #
Phox2b	407861-C2
Phox2b	407861-C3
Sox10	435931
Sox8	454781-C2
Scn7a	548561
Fabp7	414651
Pou3f1	436421-C2
MKi67	416771-C2

Interestingly, GPs in the study from Tasdemir-Yilmaz et al. (2021) were found to form three transcriptionally distinct subtypes. The g4 subtype was formed of highly proliferative cells (*Ube2c*+) from both the DRG and cochlea, although these cells were segregated within the visualization by tissue. More specialized GP from the DRG formed the g9 subtype (*Sfrp5*+), while those from the cochlea formed the g10 subtype (*Gata2*+, *Sox9*+; Tasdemir-Yilmaz et al., 2021). Nodose GP largely clustered together with the g4 subtype (Fig. 7B,C) and express high levels of *Ube2c* (Fig. 7D), indicating that they are highly proliferative (Liu et al., 2023), which makes sense given the early stage at which we sequenced nodose glial cells (P4). We found that nodose GP express the DRG GP marker *Sfrp5*, but not the cochlea GP markers *Gata2* or *Sox9* (Lilleväli et al., 2004; Veithen et al., 2023), showing that they are transcriptionally similar to DRG GP and distinct from cochlea GP (Fig. 7D).

Nodose SG were found to cluster together with g1 (DRG immature SG, iSG), g2 (DRG SG), and g5 (DRG and cochlea NMSC; Fig. 7B,C). Tasdemir-Yilmaz et al. (2021) found that SG differed between the DRG and cochlea, and our integration analysis revealed that our nodose SG largely cluster together with the g1 and g2 DRG SG subtypes. Accordingly, nodose SG express canonical SG genes shared by all SG such as *Kcnj10* and *Fgfr1*, together with genes specific to DRG SG such as *Epas1*, but not genes specific to cochlea SG such as *Srgn* (Fig. 7E; Mapps et al., 2022a). Tasdemir-Yilmaz et al. (2021)

describe the crest-derived SG subtypes g1 and g2 as having quantitative differences in gene expression, with g1 expressing the same canonical SG genes but at lower levels and likely being iSG. This is recapitulated in our nodose SG. For example, cells expressing lower levels of *Epas1*, *Glul*, and *Cxcr4* SG genes cluster together in the UMAP, indicating higher similarity, and are likely iSG (Fig. 7E, dotted circles). DRG SG express genes known to inhibit myelination such as *Ddit4* and *Ptprz1*, as DRG somas are largely unmyelinated (Kuboyama et al., 2012; Noseda et al., 2013; Nascimento et al., 2018; Tasdemir-Yilmaz et al., 2021). These genes are also expressed in nodose SG and NMSC (Fig. 7F) and might suggest that nodose somas are also largely unmyelinated. Contrastingly, cochlea SG myelinate cochlea neuron somas and share expression of many genes expressed uniquely by nodose MSC such as *Arhgap19*, *Fxyd6*, *Fa2h*, and *Gldn* (Fig. 7G; Tasdemir-Yilmaz et al., 2021).

As opposed to nodose GP and SG, nodose Schwann cells cluster together with both DRG and cochlea glial cells. Nodose MSC were found to cluster together with g6 (DRG immature Schwann cells, iSC), g7 (DRG and cochlea MSC), and g5 (DRG and cochlea NMSC; Fig. 7B,C). Similar to nodose SG showing quantitative differences in canonical SG gene expression, nodose MSCs show quantitative differences in canonical MSC gene expression, with lower expressing cells assigned to g6, iSC (Fig. 7H, dotted circles). When compared with other cells in the MSC subtype, the MSCs that are positioned in the UMAP next to NMSC

Table 3. List of all markers (antibodies and RNAscope probes), what cell types they label, and stage analyzed

|		Marker	Stage analyzed	Protein or mRNA?	Cell type
Figure 1	A	Phox2b+	E10.5–E12.5	Protein	Embryonic nodose neurons
		Sox10+	E10.5–E12.5	Protein	Embryonic nodose glial cells
		Sox10+Phoxb2+	E10.5–E12.5	Protein	Embryonic nodose glial cells
	C	GFP+	E11.5	Protein	All cells with a history of Phox2b expression
		Phox2b+	E11.5	Protein	Embryonic nodose neurons
	D	*Phox2b+*	E11.5	mRNA	Embryonic nodose neurons
		Sox10+	E11.5	mRNA	Embryonic nodose glial cells
		Sox8+	E11.5	mRNA	Schwann cell precursors
		Sox10+Phox2b+Sox8+	E11.5	mRNA	Schwann cell precursors
Extended Data Figure 1-1		Sox10+	E11.5–E12.5	Protein	Embryonic nodose glial cells
		Tlx3+	E11.5–E12.5	Protein	Embryonic nodose neurons
Figure 2	B	TrkA+	P4	Protein	Jugular neurons
		Phox2b+	P4	Protein	Nodose neurons
	C	GFP+	P4	Protein	Nodose neurons and glial cells
		Phox2b+	P4	Protein	Nodose neurons
		Sox10+	P4	Protein	Nodose glial cells
		Tlx3+	P4	Protein	Nodose neurons
	D	GFP+	P4	Protein	Jugular neurons, glial cells and nodose glial cells
		Sox10+	P4	Protein	Nodose glial cells
	F	β-gal	P4	Protein	Jugular neurons
		Tlx3+	P4	Protein	Jugular neurons
		TrkA+	P4	Protein	Jugular neurons
	G	β-gal	P4	Protein	Nodose neurons
		Tlx3+	P4	Protein	Nodose neurons
		TrkB+	P4	Protein	Nodose neurons
Figure 3	B	GFP+	P4	Protein	Nodose glial cells
		TrkA+	P4	Protein	Jugular neurons
		Phox2b+	P4	Protein	Nodose neurons
	C	GFP+	P4	Protein	Nodose glial cells
		Sox10+	P4	Protein	Jugular and nodose glial cells
	D	tdTomato+	P4	Protein	Nodose glial cells
		GFP+	P4	Protein	Jugular neurons
		β-gal	P4	Protein	Jugular neurons
Figure 4	A	tdTomato+	P4	Protein	Nodose neurons and glial cells
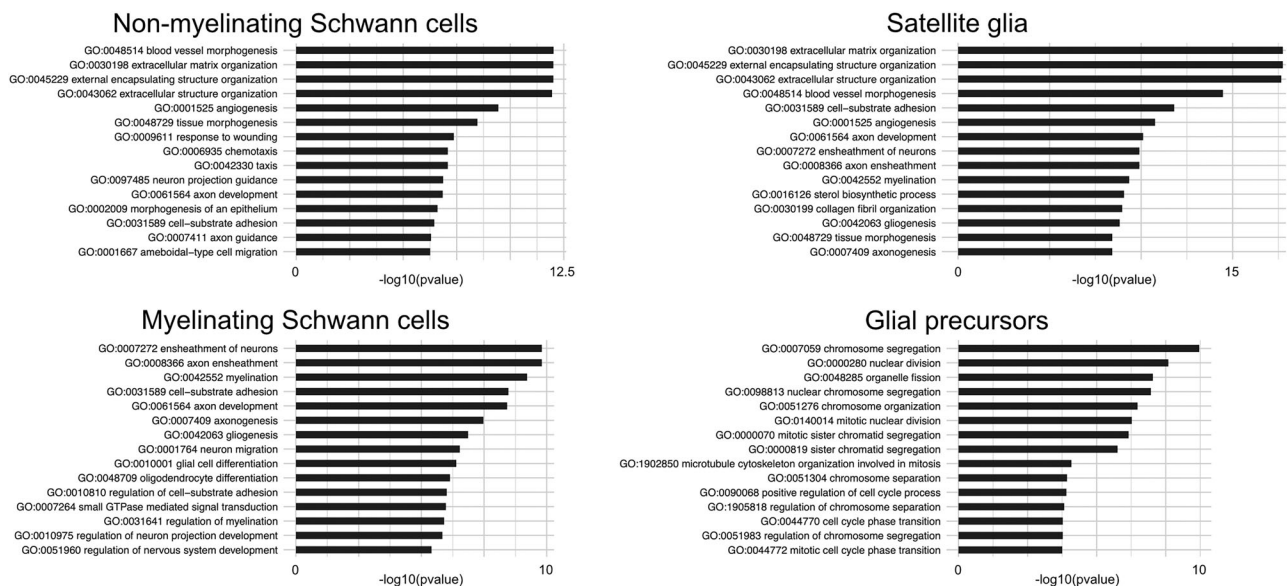
Figure 5. GO term analysis reveals putative roles for the four glial cell subtypes. Top 15 enriched GO terms for NMSCs, MSCs, SG, and GPs.

express higher levels of genes known to inhibit myelination (*Ddit4* and *Ptprz1*; Fig. 7F, dotted circles), lower levels of canonical MSC genes *Mpz* and *Prx* (Fig. 7H, dotted circles; Su et al., 1993; Gillespie et al., 2000), and higher levels of NMSC genes *L1cam* (Fig. 7I, dotted circles) and *Scn7a* (Fig. 4G). Thus, these cells likely represent iSC that generate both NMSC and MSC.
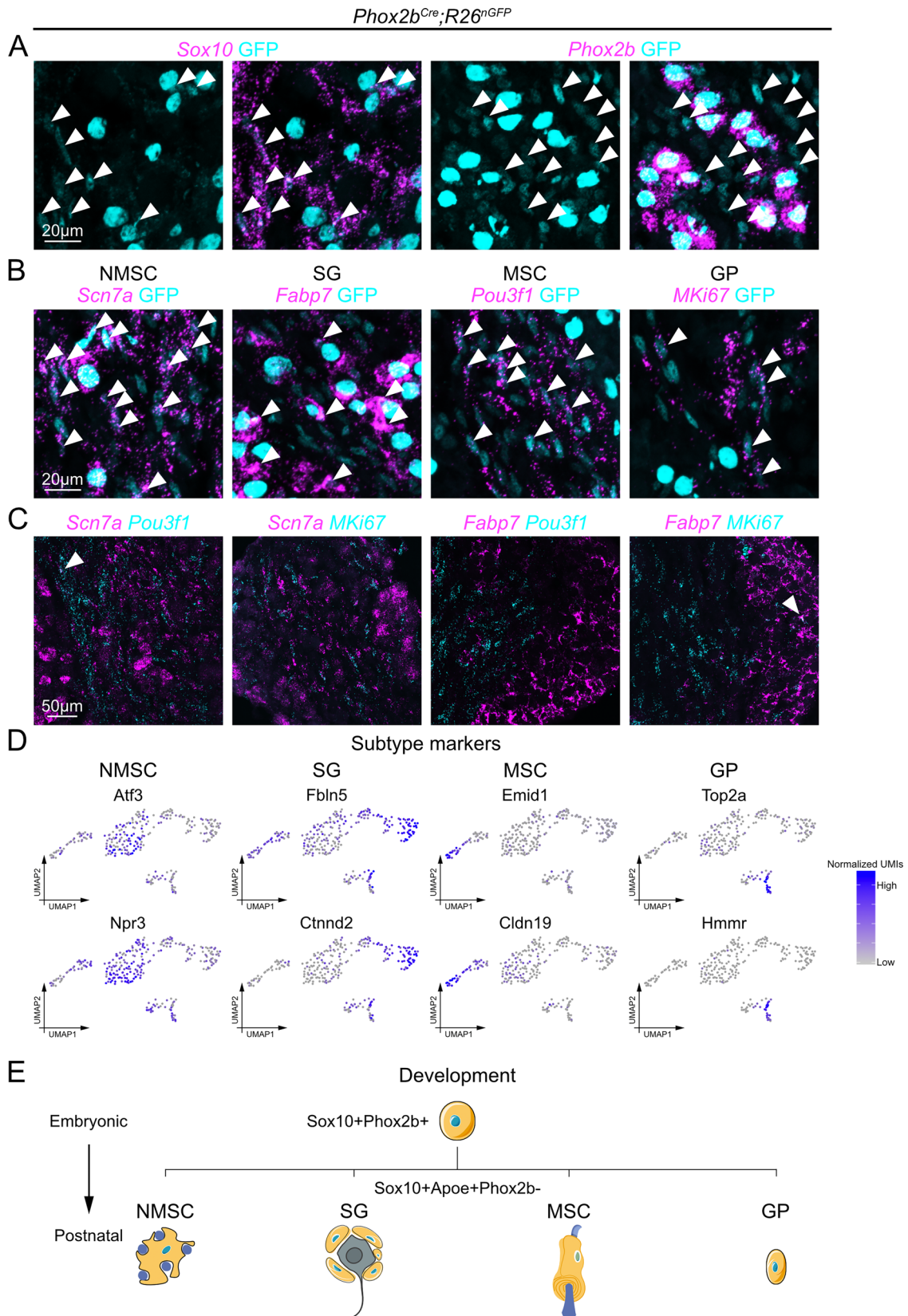
Figure 6. smFISH confirms that Sox10+Phox2b+ cells give rise to all major glial cell types in the nodose ganglia in vivo. *A*, *Phox2b^{Cre};R26^{nGFP}* mice were used to label all cells with a history of Phox2b expression with nuclear GFP (cyan). Nodose ganglia at P4 were analyzed using immunofluorescence against GFP (cyan) and smFISH probes against *Sox10* (magenta, left) to label glial cells and *Phox2b* (magenta, right) to label neurons. Notice the many GFP+ glial cells that are *Phox2b*—. Arrowheads mark GFP+ glial cells with a history of Phox2b expression that are *Sox10*+ (left) and *Phox2b*— (right). *B*, Nodose ganglia were analyzed at P4 using immunohistology against GFP (cyan) together with smFISH probes (magenta) against *Scn7a* to label NMSC, *Fabp7* to label SG, *Pou3f1* to label MSC, and *MKi67* to label GP. Arrowheads mark marker+GFP+ cells. Note that Phox2b+ nodose neurons have large, bright, and round nuclei, while glial cells with a

Lastly, all nodose NMSC clustered together with g5 (DRG and cochlea NMSC; Fig. 7B,C). Nodose NMSCs express classical NMSC genes such as *L1cam* and *Ngfr*, similar to both DRG and cochlea NMSC (Fig. 7I; Salton et al., 1983; Yasuda et al., 1987; Tasdemir-Yilmaz et al., 2021). In conclusion, by performing an integration analysis and combining our scRNA-seq data together with that of Tasdemir-Yilmaz et al. (2021), we found unexplored immature glial subtypes in our dataset. This finding was supported by the fact that nodose GP contributed cells to g1 (iSG cells), g5 (NMSCs), and g6 (iSC).

Discussion

The cranial neural crest generates the peripheral glial cells that populate the nodose ganglia and support resident viscerosensory neurons in their homeostatic functions. Here, we show that some Sox10+ neural crest-derived precursors transiently express Phox2b, before populating the nodose, but not the jugular ganglia, with glial cells. Glial derivatives from the Sox10+Phox2b+ neural crest progenitors include MSCs and NMSCs, as well as SG and GPs. scRNA-seq revealed the transcriptomic signatures of these four major glial cell types, which we confirm derive from progenitors with a history of Phox2b expression. Our work demonstrates the existence of a novel cranial neural crest progenitor population, namely, nerve-associated Sox10 +Phox2b+ cells, that generate the entire repertoire of nodose, but not jugular, glial subtypes.

Nodose glial cell development

From the discovery of the neural crest by His in 1868, this progenitor niche has captured the attention of generations of scientists given the vast multitude of cell types that it generates (His, 1868; Dupont, 2018; Tang and Bronner, 2020). The cranial neural crest gives rise to many different cells that populate the head and face region in vertebrates, including the bone, cartilage, melanocytes, as well as sensory neurons and glial cells (Le Douarin et al., 2004; Erickson et al., 2023). Until the development of quail–chick transplantation as a means of tracing the derivatives from different embryonic progenitor zones, there was much debate over the exact development of cranial sensory ganglia (Le Douarin, 1986). The generation of nodose ganglia was particularly controversial, and it was only in 1980 that its glial component was definitively shown to derive from the neural crest and its neurons from the epibranchial placode (Narayanan and Narayanan, 1980).

Although the same cranial neural crest gives rise to glial cells in both the nodose and the neighboring jugular ganglia, it is only in the nodose ganglia where some glial cells have a history of transient Phox2b expression (Fig. 3). Transient Phox2b expression in Sox10 + cells has been described in other crest-derived progenitors that choose between neuronal and glial fates such as in enteric and parasympathetic ganglia (Dyachuk et al., 2014; Espinosa-Medina et al., 2014, 2017; Soldatov et al., 2019). In contrast to these other autonomic structures that derive their neuronal and glial components from the neural crest, the neural crest only contributes glial cells to the nodose ganglia. Recent scRNA-seq studies revealed that in

the neural crest, cell fate is decided by a series of binary decisions between competing transcriptional programs (Soldatov et al., 2019; Faure et al., 2020). Thus, Phox2b is expressed early in autonomic crest progenitors that differentiate into neurons and glial cells, but its expression is quickly downregulated in glial cells and only maintained in neurons (Dyachuk et al., 2014; Espinosa-Medina et al., 2014). Why Phox2b, a master regulator of autonomic cell fate, is expressed in the cranial neural crest progenitors that generate Phox2b− glial cells in the nodose ganglia was not immediately apparent.

It is now known that sympathetic and enteric, but not somatosensory, neurons depend on Phox2b for their development (Pattyn et al., 1999; Espinosa-Medina et al., 2017; Soldatov et al., 2019). Furthermore, nerve-associated crest progenitors along the vagus nerve generate Phox2b+ neurons that reside in esophageal and stomach enteric ganglia (Espinosa-Medina et al., 2017). Lastly, genetic studies showed that Phox2b suppresses somatosensory fates in favor of viscerosensory ones (D'Autréaux et al., 2011). Thus, it seems as though the crest-derived Sox10 +Phox2b+ progenitors that give rise to nodose glial cells described here are part and parcel of the same population of crest-derived cells that have the potential to generate other Phox2b+ autonomic neurons, but not Phox2b− somatosensory neurons. We captured the Sox10+Phox2b+ cells at a cross-roads, deciding between turning off Phox2b expression to generate the full complement of nodose glial cells and maintaining Phox2b expression and continuing to travel along the vagus nerve to generate sympathetic or enteric neurons.

One of the major questions regarding the multipotent neural crest is whether cell fates are determined intrinsically based on their lineage or if extrinsic factors also play a role (Le Douarin, 1986). A quail–chick transplantation study by Ayer-le Lievre and Le Douarin addressed this question by grafting quail crest into a chick host, letting the host develop, and then removing the chimeric nodose ganglia and back-transplanting it into the cranial neural crest of a younger chick host (Ayer-Le Lievre and Le Douarin, 1982). When they examined the chick hosts that received chimeric quail–chick nodose ganglia grafts, they found quail cells in numerous sympathetic and enteric, but not somatosensory, ganglia (Ayer-Le Lievre and Le Douarin, 1982). Thus, the cranial neural crest that in vivo only generates nodose glial cells contains numerous "unused" autonomic neural potentialities, demonstrating that extrinsic factors play a role in neural crest fate selection.

The transient expression of Phox2b in some Sox10+ crest-derived progenitors that generate nodose, but not jugular, glial cells might be due to environmental differences. For instance, transient expression of Phox2b in nodose glial cells could be induced by interactions with other Phox2b+ cells such as viscerosensory or visceromotor neurons that form the vagus nerve or placodal neuronal progenitors as they travel to the nodose anlage. Although the mechanism governing Phox2b expression in crest-derived nodose glial cells is unclear, the "unused" fates of the crest cells described by Ayer-le Lievre and Le Douarin that become available in a new environment are only those that depend on the expression of Phox2b.

---

history of Phox2b expression have smaller, dimmer, oblong-shaped nuclei. *C*, smFISH with probes against glial subtype markers show that there is hardly any overlap between glial subtypes. Arrowheads label rare cells that simultaneously express subtype markers for two glial subtypes. *C*, UMAPs showing additional subtype marker genes for NMSCs, SG, MSCs, and GPs. *D*, Summary diagram showing that Sox10+Phox2b+ cells during early development give rise to Sox10+Apoe+Phox2b− NMSC, SG, MSC, and GP postnatally. Illustrations were adapted from bioicons.com and scidraw.io and licensed under CC-BY 3.0 and CC-BY 4.0.
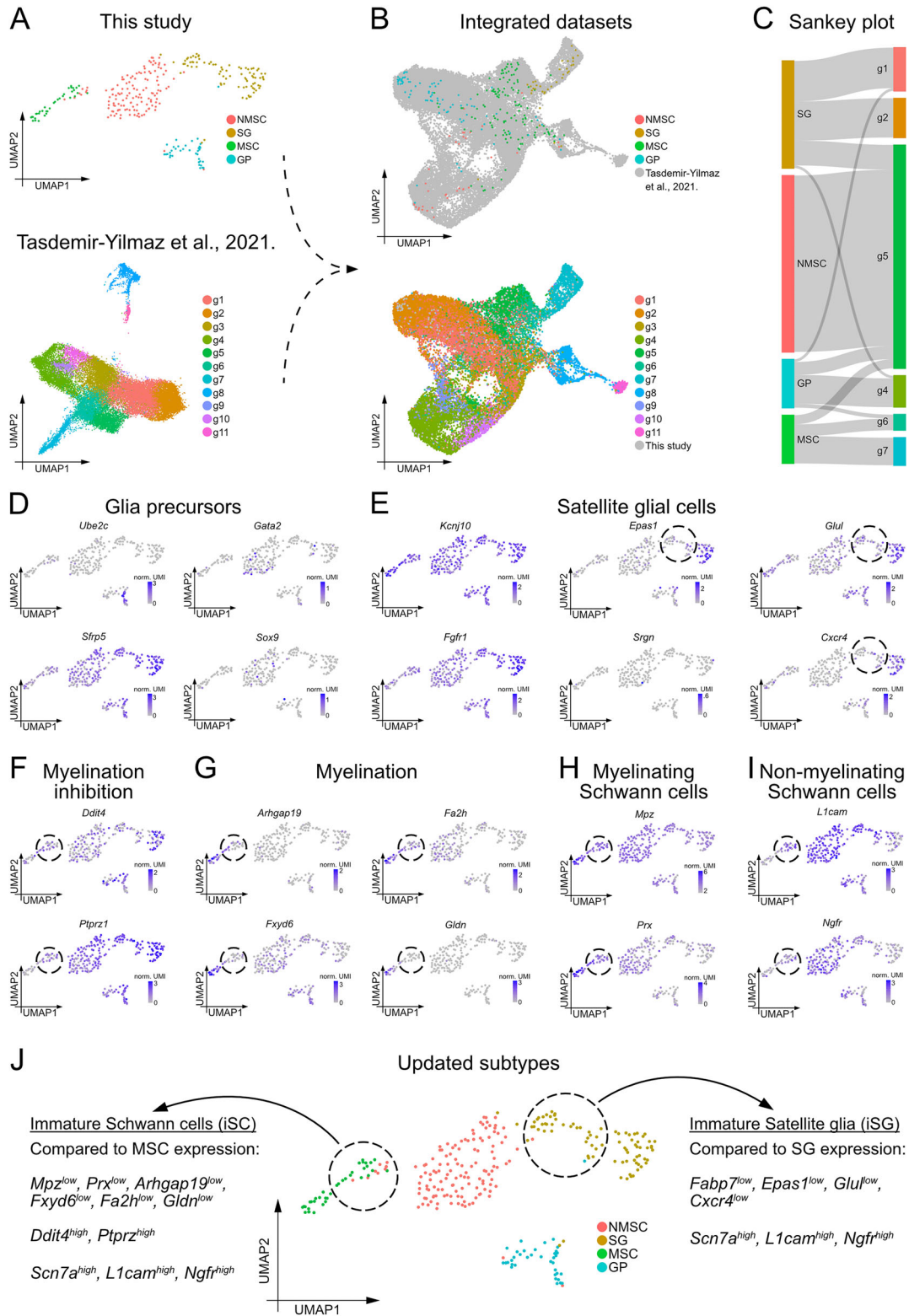
Figure 7. Dataset integration of peripheral glial cells reveals transcriptomic similarities between DRG and nodose ganglia glial cells. **A**, Top, UMAP plot of nodose glial cells, with each subtype labeled in a different color. The UMAP plot revealed four transcriptomically unique non-neuronal subtypes: NMSCs (peach), SG (gold), MSCs (green), and GPs (blue). Bottom, 2D visualization of glial subtypes g1–g11 from Tasdemir-Yilmaz et al. (2021). **B**, UMAP of the integration analysis between the datasets shown in **A**. Top, nodose glial cells are shown color-coded by subtype, with the Tasdemir-Yilmaz et al. (2021) glial cells shown in gray. Bottom, Tasdemir-Yilmaz et al. (2021) glial cells are shown color-coded by subtype, with nodose glial cells shown in gray. **C**, Sankey plot that displays the results from Suerat's cell-type label transfer assigning the labels of the reference dataset [Tasdemir-Yilmaz et al. (2021) glial subtypes] to the cells of the query dataset (nodose glial subtypes). **D**, UMAP plots of nodose glial cells for GP genes *Ube2c*, *Gata2*, *Sfrp5*, and *Sox9*. **E**, UMAP plots of nodose glial cells for SG genes *kcnj10*, *Fgfr1*, *Epas1*, *Srgn*, *Glul*, and *Cxcr4*. iSG are shown with the dotted circles. **F**, UMAP plots of nodose glial cells for genes known to inhibit myelination: *Ddit4* and *Ptprz1*. iSC are shown with the dotted circles. **G**, UMAP plots of nodose glial cells for genes expressed in cochlea SG that are expressed in MSC: *Arhgap19*, *Fxyd6*, *Fa2h*, and *Gldn*. iSC are shown with the dotted circle. **H**, UMAP plots of nodose glial cells for MSC genes *Mpz* and *Prx*. iSC are shown with the dotted circles. **I**, UMAP plots of nodose glial cells for NMSC genes *L1cam* and *ngfr*. iSC are shown with the dotted circles. **J**, A UMAP plot of nodose glial cells, with each subtype labeled in a different color. Dotted circles show iSC (left) and iSG (right), with marker genes listed.

Having demonstrated the developmental origin and potential fates of Sox10+Phox2b+ cells within the nodose ganglia, our work opens up avenues for future studies to probe the functional relevance of transient Phox2b expression in the Sox10+ crest-derived progenitors that generate nodose glial cells. Indeed, previous studies in other crest derivatives have shown that Sox10 and Phox2b can compete and reciprocally inhibit each other to bias differentiation toward either a glial or neuronal fate, respectively (Kim et al., 2003; Nagashimada et al., 2012; Soldatov et al., 2019; Kastriti et al., 2022; Erickson et al., 2023). Here, we show that Sox10 and Phox2b are coexpressed in nodose glial derivatives during early development, and it would be of interest to causally test whether Phox2b expression is functionally relevant for cell fate choice by either ablating or overexpressing Phox2b. We predict that if Phox2b is ablated in the neural crest, there would be an increase in nodose glial cells, with a concomitant decrease in enteric and/or autonomic neurons, whereas overexpression of Phox2b in the neural crest would have the opposite effect.

Glial cell diversity

The development of scRNA-seq has uncovered the remarkable heterogeneity of cell types contained within the central and peripheral nervous systems. More recently, this technique has revealed glial heterogeneity in peripheral nerves such as the brachial plexus and sciatic nerve, as well as in peripheral ganglia such as the DRG, spiral ganglia, and superior cervical ganglia (Wolbert et al., 2020; Tasdemir-Yilmaz et al., 2021; Avraham et al., 2022; Mapps et al., 2022b). While the glial cell types found in peripheral nerves only consist of MSCs and NMSCs, peripheral ganglia also include SG cells (Jessen and Mirsky, 2005). These different types of peripheral glial cells work to provide trophic support and myelination to neurons in the peripheral nervous system (Jessen and Mirsky, 2005; Jessen et al., 2015; Hanani and Spray, 2020). Here, we show that neural crest-derived Sox10+Phox2b+ progenitors give rise to SG and GPs, in addition to Schwann cells.

While recent studies profiled the transcriptomes of glial cells found in sympathetic, auditory, and somatosensory ganglia (Tasdemir-Yilmaz et al., 2021; Mapps et al., 2022b), here we sequenced glial cells from the viscerosensory nodose ganglia. We used the scRNA-seq data from Tasdemir-Yilmaz et al. (2021) to perform an integration analysis, revealing subpopulations of iSG cells and iSC that were previously hidden in our nodose glial cell dataset, demonstrating the utility of performing integration analyses with other published datasets (Fig. 7J). Interestingly, our dataset integration revealed that nodose GPs and SG are more transcriptomically similar to those from the DRG than those from the cochlea. On the other hand, nodose, DRG, and cochlea Schwann cells, including both myelinating and nonmyelinating subtypes, seem to share a core transcriptional program, despite the marked differences between the viscerosensory, somatosensory, and auditory neurons contained within these distinct ganglia.

References

Abe T, Kiyonari H, Shioi G, Inoue K-I, Nakao K, Aizawa S, Fujimori T (2011) Establishment of conditional reporter mouse lines at ROSA26 locus for live cell imaging. Genesis 49:579–590.

Adameyko I, et al. (2012) Sox2 and Mitf cross-regulatory interactions consolidate progenitor and melanocyte lineages in the cranial neural crest. Development 139:397–410.

Avraham O, Chamessian A, Feng R, Yang L, Halevi AE, Moore AM, Gereau RW, Cavalli V (2022) Profiling the molecular signature of satellite glial cells at the single cell level reveals high similarities between rodents and humans. Pain 163:2348–2364.

Avraham O, Deng P-Y, Jones S, Kuruvilla R, Semenkovich CF, Klyachko VA, Cavalli V (2020) Satellite glial cells promote regenerative growth in sensory neurons. Nat Commun 11:4891.

Ayer-Le Lievre CS, Le Douarin NM (1982) The early development of cranial sensory ganglia and the potentialities of their component cells studied in quail-chick chimeras. Dev BIiol 94:291–310.

Bermingham JR, Scherer SS, O'Connell S, Arroyo E, Kalla KA, Powell FL, Rosenfeld MG (1996) Tst-1/Oct-6/SCIP regulates a unique step in peripheral myelination and is required for normal respiration. Genes Dev 10:1751–1762.

Boyles JK, Pitas RE, Wilson E, Mahley RW, Taylor JM (1985) Apolipoprotein E associated with astrocytic glia of the central nervous system and with nonmyelinating glia of the peripheral nervous system. J Clin Invest 76:1501–1513.

Breuskin I, Bodson M, Thelen N, Thiry M, Borgs L, Nguyen L, Stolt C, Wegner M, Lefebvre PP, Malgrange B (2010) Glial but not neuronal development in the cochleo-vestibular ganglion requires Sox10. J Neurochem 114:1827–1839.

Britsch S, Goerich DE, Riethmacher D, Peirano RI, Rossner M, Nave K-A, Birchmeier C, Wegner M (2001) The transcription factor Sox10 is a key regulator of peripheral glial development. Genes Dev 15:66–78.

Chang RB, Strochlic DE, Williams EK, Umans BD, Liberles SD (2015) Vagal sensory neuron subtypes that differentially control breathing. Cell 161:622–633.

D'amico-Martel A, Noden DM (1983) Contributions of placodal and neural crest cells to avian cranial peripheral ganglia. Am J Anat 166:445–468.

Danielian PS, Muccino D, Rowitch DH, Michael SK, McMahon AP (1998) Modification of gene activity in mouse embryos in utero by a tamoxifen-inducible form of Cre recombinase. Curr Biol 8:1323–S2.

D'Autréaux F, Coppola E, Hirsch M-R, Birchmeier C, Brunet J-F (2011) Homeoprotein Phox2b commands a somatic-to-visceral switch in cranial sensory pathways. Proc Natl Acad Sci U S A 108:20018–20023.

Dobin A, Davis CA, Schlesinger F, Drenkow J, Zaleski C, Jha S, Batut P, Chaisson M, Gingeras TR (2013) STAR: ultrafast universal RNA-seq aligner. Bioinformatics 29:15–21.

Dorsky RI, Moon RT, Raible DW (1998) Control of neural crest cell fate by the Wnt signalling pathway. Nature 396:370–373.

Douarin NL, Dulac C, Dupin E, Cameron-Curry P (1991) Glial cell lineages in the neural crest. Glia 4:175–184.

Duan R-S, Jin T, Yang X, Mix E, Adem A, Zhu J (2007) Apolipoprotein E deficiency enhances the antigen-presenting capacity of Schwann cells. Glia 55:772–776.

Dupont J-C (2018) Historical perspective on neuroembryology: Wilhelm His and his contemporaries. Genesis 56:e23218.

Dyachuk V, et al. (2014) Parasympathetic neurons originate from nerve-associated peripheral glial progenitors. Science 345:82–87.

Erickson AG, Kameneva P, Adameyko I (2023) The transcriptional portraits of the neural crest at the individual cell level. Semin Cell Dev Biol 138:68–80.

Espinosa-Medina I, Jevans B, Boismoreau F, Chettouh Z, Enomoto H, Müller T, Birchmeier C, Burns AJ, Brunet J-F (2017) Dual origin of enteric neurons in vagal Schwann cell precursors and the sympathetic neural crest. Proc Natl Acad Sci U S A 114:11980–11985.

Espinosa-Medina I, Outin E, Picard CA, Chettouh Z, Dymecki S, Consalez GG, Coppola E, Brunet J-F (2014) Parasympathetic ganglia derive from Schwann cell precursors. Science 345:87–90.

Faure L, et al. (2020) Single cell RNA sequencing identifies early diversity of sensory neurons forming via bi-potential intermediates. Nat Commun 11:4175.

Fields RD, Burnstock G (2006) Purinergic signalling in neuron–glia interactions. Nat Rev Neurosci 7:423–436.

Fode C, Gradwohl G, Morin X, Dierich A, LeMeur M, Goridis C, Guillemot F (1998) The bHLH protein NEUROGENIN 2 is a determination factor for epibranchial placode–derived sensory neurons. Neuron 20:483–494.

Fontaine-Perus J, Chanconie M, Le Douarin NM (1988) Developmental potentialities in the nonneuronal population of quail sensory ganglia. Dev Biol 128:359–375.

Furlan A, et al. (2017) Multipotent peripheral glial cells generate neuroendocrine cells of the adrenal medulla. Science 357:eaal3753.

Gavin BJ, McMahon JA, McMahon AP (1990) Expression of multiple novel Wnt-1/int-1-related genes during fetal and adult mouse development. Genes Dev 4:2319–2332.

Gerber D, Pereira JA, Gerber J, Tan G, Dimitrieva S, Yánguez E, Suter U (2021) Transcriptional profiling of mouse peripheral nerves to the single-cell level to build a sciatic nerve ATlas (SNAT). eLife 10:e58591.

Gillespie CS, et al. (2000) Peripheral demyelination and neuropathic pain behavior in periaxin-deficient mice. Neuron 26:523–531.

Hanani M (2005) Satellite glial cells in sensory ganglia: from form to function. Brain Res Rev 48:457–476.

Hanani M, Spray DC (2020) Emerging importance of satellite glia in nervous system function and dysfunction. Nat Rev Neurosci 21:485–498.

Hanani M, Verkhratsky A (2021) Satellite glial cells and astrocytes, a comparative review. Neurochem Res 46:2525–2537.

Hao Y, (2021) Integrated analysis of multimodal single-cell data. Cell 184:3573–3587.e29.

Harty BL, Monk KR (2017) Unwrapping the unappreciated: recent progress in Remak Schwann cell biology. Curr Opin Neurobiol 47:131–137.

Hashimshony T, et al. (2016) CEL-Seq2: sensitive highly-multiplexed single-cell RNA-Seq. Genome Biol 17:77.

Hippenmeyer S, Vrieseling E, Sigrist M, Portmann T, Laengle C, Ladle DR, Arber S (2005) A developmental switch in the response of DRG neurons to ETS transcription factor signaling. PLoS Biol 3:e159.

Hirsch M-R, d'Autréaux F, Dymecki SM, Brunet J-F, Goridis C (2013) A Phox2b::FLPo transgenic mouse line suitable for intersectional genetics: transgenic line Phox2b::FLPo. Genesis 51:506–514.

His W (1868) Untersuchungen über die erste Anlage des Wirbelthierleibes: Die erste Entwicklung des Hühnchens im Ei.

Jacob C (2015) Transcriptional control of neural crest specification into peripheral glia: control of peripheral glia specification. Glia 63:1883–1896.

Jaegle M, Mandemakers W, Broos L, Zwart R, Karis A, Visser P, Grosveld F, Meijer D (1996) The POU factor Oct-6 and Schwann cell differentiation. Science 273:507–510.

Jessen KR, Mirsky R (2005) The origin and development of glial cells in peripheral nerves. Nat Rev Neurosci 6:671–682.

Jessen KR, Mirsky R, Lloyd AC (2015) Schwann cells: development and role in nerve repair. Cold Spring Harb Perspect Biol 7:a020487.

Kastriti ME, et al. (2022) Schwann cell precursors represent a neural crest-like state with biased multipotency. EMBO J 41:e108780.

Kim J, Lo L, Dormand E, Anderson DJ (2003) SOX10 maintains multipotency and inhibits neuronal differentiation of neural crest stem cells. Neuron 38:17–31.

Kondo T, Sheets PL, Zopf DA, Aloor HL, Cummins TR, Chan RJ, Hashino E (2008) Tlx3 exerts context-dependent transcriptional regulation and promotes neuronal differentiation from embryonic stem cells. Proc Natl Acad Sci U S A 105:5780–5785.

Kuboyama K, Fujikawa A, Masumura M, Suzuki R, Matsumoto M, Noda M (2012) Protein tyrosine phosphatase receptor type z negatively regulates oligodendrocyte differentiation and myelination. PLoS One 7: e48797.

Kuhlbrodt K, Herbarth B, Sock E, Hermans-Borgmeyer I, Wegner M (1998) Sox10, a novel transcriptional modulator in glial cells. J Neurosci 18:237–250.

Kupari J, Häring M, Agirre E, Castelo-Branco G, Ernfors P (2019) An atlas of vagal sensory neurons and their molecular specialization. Cell Rep 27: 2508–2523.e4.

Kurtz A, Zimmer A, Schnütgen F, Brüning G, Spener F, Müller T (1994) The expression pattern of a novel gene encoding brain-fatty acid binding protein correlates with neuronal and glial cell development. Development 120:2637–2649.

Le Douarin NM (1986) Cell line segregation during peripheral nervous system ontogeny. Science 231:1515–1522.

Le Douarin NM, Creuzet S, Couly G, Dupin E (2004) Neural crest cell plasticity and its limits. Development 131:4637–4650.

Lilleväli K, Matilainen T, Karis A, Salminen M (2004) Partially overlapping expression of Gata2 and Gata3 during inner ear development. Dev Dyn 231:775–781.

Liu W, et al. (2023) Lactate regulates cell cycle by remodelling the anaphase promoting complex. Nature 616:790–797.

Lowenstein ED, et al. (2023) Prox2 and Runx3 vagal sensory neurons regulate esophageal motility. Neuron 111:2184–2200.e7.

Madisen L, et al. (2010) A robust and high-throughput Cre reporting and characterization system for the whole mouse brain. Nat Neurosci 13:133–140.

Madisen L, et al. (2015) Transgenic mice for intersectional targeting of neural sensors and effectors with high specificity and performance. Neuron 85: 942–958.

Mapps AA, et al. (2022a) Satellite glia modulate sympathetic neuron survival, activity, and autonomic function. eLife 11:e74295.

Mapps AA, Thomsen MB, Boehm E, Zhao H, Hattar S, Kuruvilla R (2022b) Diversity of satellite glia in sympathetic and sensory ganglia. Cell Rep 38: 110328.

Monk KR, Feltri ML, Taveggia C (2015) New insights on Schwann cell development. Glia 63:1376–1393.

Morin X, Cremer H, Hirsch MR, Kapur RP, Goridis C, Brunet JF (1997) Defects in sensory and autonomic ganglia and absence of locus coeruleus in mice deficient for the homeobox gene Phox2a. Neuron 18:411–423.

Müller T, Anlag K, Wildner H, Britsch S, Treier M, Birchmeier C (2005) The bHLH factor Olig3 coordinates the specification of dorsal neurons in the spinal cord. Genes Dev 19:733–743.

Nagashimada M, Ohta H, Li C, Nakao K, Uesaka T, Brunet J-F, Amiel J, Trochet D, Wakayama T, Enomoto H (2012) Autonomic neurocristopathy-associated mutations in PHOX2B dysregulate Sox10 expression. J Clin Invest 122:3145–3158.

Narayanan CH, Narayanan Y (1980) Neural crest and placodal contributions in the development of the glossopharyngeal-vagal complex in the chick. Anat Rec 196:71–82.

Nascimento AI, Mar FM, Sousa MM (2018) The intriguing nature of dorsal root ganglion neurons: linking structure with polarity and function. Prog Neurobiol 168:86–103.

Nassenstein C, Taylor-Clark TE, Myers AC, Ru F, Nandigama R, Bettner W, Undem BJ (2010) Phenotypic distinctions between neural crest and placodal derived vagal C-fibres in mouse lungs: vagal C-fibre subtypes innervating the lung. J Physiol 588:4769–4783.

Noseda R, et al. (2013) DDIT4/REDD1/RTP801 is a novel negative regulator of Schwann cell myelination. J Neurosci 33:15295–15305.

Pattyn A, Morin X, Cremer H, Goridis C, Brunet J-F (1997) Expression and interactions of the two closely related homeobox genes Phox2a and Phox2b during neurogenesis. Development 124:4065–4075.

Pattyn A, Morin X, Cremer H, Goridis C, Brunet J-F (1999) The homeobox gene Phox2b is essential for the development of autonomic neural crest derivatives. Nature 399:366–370.

Prescott SL, Liberles SD (2022) Internal senses of the vagus nerve. Neuron 110:579–599.

Riethmacher D, Sonnenberg-Riethmacher E, Brinkmann V, Yamaai T, Lewin GR, Birchmeier C (1997) Severe neuropathies in mice with targeted mutations in the ErbB3 receptor. Nature 389:725–730.

Salton SR, Richter-Landsberg C, Greene LA, Shelanski ML (1983) Nerve growth factor-inducible large external (NILE) glycoprotein: studies of a central and peripheral neuronal marker. J Neurosci 3:441–454.

Soldatov R, et al. (2019) Spatiotemporal structure of cell fate decisions in murine neural crest. Science 364:eaas9536.

Stam FJ, Hendricks TJ, Zhang J, Geiman EJ, Francius C, Labosky PA, Clotman F, Goulding M (2012) Renshaw cell interneuron specialization is controlled by a temporally restricted transcription factor program. Development 139:179–190.

Su Y, Brooks DG, Li L, Lepercq J, Trofatter JA, Ravetch JV, Lebo RV (1993) Myelin protein zero gene mutated in Charcot-Marie-tooth type 1B patients. Proc Natl Acad Sci U S A 90:10856–10860.

Tang W, Bronner ME (2020) Neural crest lineage analysis: from past to future trajectory. Development 147:dev193193.

Tasdemir-Yilmaz OE, et al. (2021) Diversity of developing peripheral glia revealed by single-cell RNA sequencing. Dev Cell 56:2516–2535.e8.

Véga C, Martiel J, Drouhault D, Burckhart M, Coles JA (2003) Uptake of locally applied deoxyglucose, glucose and lactate by axons and Schwann cells of rat vagus nerve. J Physiol 546:551–564.

Veithen M, Huyghe A, Van Den Ackerveken P, Fukada S-I, Kokubo H, Breuskin I, Nguyen L, Delacroix L, Malgrange B (2023) Sox9 inhibits cochlear hair cell fate by upregulating Hey1 and HeyL antagonists of Atoh1. Cells 12:2148.

Vermeiren S, Bellefroid EJ, Desiderio S (2020) Vertebrate sensory ganglia: common and divergent features of the transcriptional programs generating their functional specialization. Front Cell Dev Biol 8:587699.

Watanabe E, Hiyama TY, Kodama R, Noda M (2002) Nax sodium channel is expressed in non-myelinating Schwann cells and alveolar type II cells in mice. Neurosci Lett 330:109–113.

Wolbert J, et al. (2020) Redefining the heterogeneity of peripheral nerve cells in health and autoimmunity. Proc Natl Acad Sci U S A 117: 9466–9476.

Wu J, Saint-Jeannet J-P, Klein PS (2003) Wnt-frizzled signaling in neural crest formation. Trends Neurosci 26:40–45.

Yang C, Kim H-S, Seo H, Kim C-H, Brunet J-F, Kim K-S (2002) Paired-like homeodomain proteins, Phox2a and Phox2b, are responsible for noradrenergic cell-specific transcription of the dopamine β-hydroxylase gene. J Neurochem 71:1813–1826.

Yasuda T, Sobue G, Mokuno K, Kreider B, Pleasure D (1987) Cultured rat Schwann cells express low affinity receptors for nerve growth factor. Brain Res 436:113–119.

Zeng W-Z, Marshall KL, Min S, Daou I, Chapleau MW, Abboud FM, Liberles SD, Patapoutian A (2018) PIEZOs mediate neuronal sensing of blood pressure and the baroreceptor reflex. Science 362:464–467.

Zhou Y, et al. (2019) PMP22 regulates cholesterol trafficking and ABCA1-mediated cholesterol efflux. J Neurosci 39:5404–5418.

Zou D, Silvius D, Fritzsch B, Xu P-X (2004) Eya1 and Six1 are essential for early steps of sensory neurogenesis in mammalian cranial placodes. Development 131:5561–5572.